SyNPL: Synthetic Notch pluripotent cell lines to monitor and manipulate cell interactions *in vitro* and *in vivo*.

Running title: Engineering cell interactions

Mattias Malaguti[1,‡], Rosa Portero Migueles[1], Jennifer Annoh[1], Daina Sadurska[1,2], Guillaume Blin[1], Sally Lowell[1,‡]

1. Centre for Regenerative Medicine, Institute for Stem Cell Research, School of Biological Sciences, University of Edinburgh, 5 Little France Drive, Edinburgh EH16 4UU, UK
2. Current address: Sir William Dunn School of Pathology, University of Oxford, Oxford, United Kingdom

‡ Authors for correspondence: mattias.malaguti@ed.ac.uk sally.lowell@ed.ac.uk

Keywords: Cell interaction; SynNotch; pluripotent stem cells; cell engineering, patterning.

SUMMARY STATEMENT

Optimised Synthetic Notch circuitry in mouse pluripotent stem cells provides a modular tool to monitor cell-cell interactions and program synthetic patterning of cell fates in culture and in embryos.

ABSTRACT

Cell-cell interactions govern differentiation and cell competition in pluripotent cells during early development, but the investigation of such processes is hindered by a lack of efficient analysis tools. Here we introduce SyNPL: clonal pluripotent stem cell lines which employ optimised Synthetic Notch (SynNotch) technology to report cell-cell interactions between engineered "sender" and "receiver" cells in cultured pluripotent cells and chimaeric mouse embryos. A modular design makes it straightforward to adapt the system for programming differentiation decisions non-cell-autonomously in receiver cells in response to direct contact with sender cells. We demonstrate the utility of this system by enforcing neuronal differentiation at the boundary between two cell populations. In summary, we provide a new tool which could be used to identify cell interactions and to profile changes in gene or protein expression that result from direct cell-cell contact with defined cell populations in culture and in early embryos, and which can be adapted to generate synthetic patterning of cell fate decisions.

INTRODUCTION

During embryogenesis, pluripotent cells undergo a series of cell fate decisions that are controlled by interactions between epiblast cells, their early differentiated derivatives, and the surrounding extraembryonic tissues (Arnold and Robertson, 2009; Nowotschin and Hadjantonakis, 2010; Rossant and Tam, 2009). The transcriptional changes that accompany exit from pluripotency and differentiation into specific cell types have been extensively characterised, and the long-range signals that control these changes are now well understood (De Los Angeles et al., 2015; Kinoshita and Smith, 2018; Pera and Tam, 2010; Posfai et al., 2021; Tam and Loebel, 2007). Less is known about how early developmental decisions are influenced by direct interactions of cells with their neighbours. It is well established that cell-cell interactions play a key role in development (Dias et al., 2014; Gurdon, 1987; Johnson and Ziomek, 1983; Schultz, 1985), but until recently there has been a paucity of molecular and technological tools available to study these processes in detail in relevant settings (Nishida-Aoki and Gujral, 2019; Yang et al., 2021).

Quantitative image analysis can be used to identify and infer the effect of neighbours on the properties of cells of interest in fixed samples (Blin et al., 2018; Fischer et al., 2020; Forsyth et al., 2021; Toth et al., 2018). We have recently developed a software suite for automated neighbour identification during live imaging (Blin et al., 2019), which provides researchers with a further dimension to study the effects on cell-cell interactions on cell fate decisions. Whilst live image analysis provides high-resolution visual information, this approach is labour-intensive and only leads to neighbour identification *a posteriori*.

The nascent field of Synthetic Developmental Biology (Davies, 2017; Ebrahimkhani and Ebisuya, 2019; Ho and Morsut, 2021; Santorelli et al., 2019; Schlissel and Li, 2020) seeks to understand the mechanisms of patterning and cell differentiation through the engineering of genetic circuits (Cachat et al., 2016; Matsuda et al., 2015; Sekine et al., 2018). By re-engineering the Notch/Delta signalling cascade (Figure 1A), Lim and colleagues generated a synthetic circuit capable of reporting and manipulating cell-cell interactions in real time (Morsut et al., 2016). In this system, a "sender" cell presenting an extracellular membrane-bound antigen of interest is recognised by a "receiver" cell expressing a chimaeric Synthetic Notch (SynNotch) receptor, composed of an extracellular antigen-recognition domain, the Notch1 core transmembrane domain containing proteolytic cleavage sites, and an intracellular synthetic effector domain (Fig. 1B-D). Thanks to the modularity of the SynNotch

64 circuitry, it is therefore possible to interrogate and manipulate the effects of interactions between cell
65 types of interest.

66 SynNotch technology has been used for monitoring cell-cell interactions, generating synthetic
67 patterns, generating synthetic morphogen gradients, inducing contact-mediated gene editing, and
68 generating custom antigen receptor T-cells (Cho et al., 2018; Choe et al., 2021; He et al., 2017; Huang
69 et al., 2020; Roybal et al., 2016; Sgodda et al., 2020; Toda et al., 2018; Toda et al., 2020; Wang et al.,
70 2021). SynNotch technology has been established in *Drosophila* (He et al., 2017) as well as in
71 immortalised cell lines and differentiated cell types, but its potential in the study of mammalian
72 developmental events remains largely untapped.

73 Mouse embryonic stem cells (ESCs) can be differentiated into any cell type of interest *in vitro*, can give
74 rise to chimaeric embryos and can be used to establish transgenic mouse lines (Bradley et al., 1984;
75 Evans and Kaufman, 1981; Martin, 1981). Adapting the SynNotch system for use in mouse ESCs would
76 therefore permit monitoring and manipulation of cell-cell interactions in a developmental context
77 both *in vivo* and *in vitro*. The original system designed by (Morsut et al., 2016) used lentiviral
78 transduction of immortalised and primary cell lines, where transgene expression was driven from the
79 retroviral SFFV promoter. Lentiviral transduction can lead to multiple copy transgene integration in
80 mouse ESCs (Pfeifer et al., 2002), and the SFFV promoter is prone to silencing in mouse pluripotent
81 cells and their derivatives (Herbst et al., 2012; Pfaff et al., 2013; Wu et al., 2011), making this system
82 suboptimal for mouse ESCs.

83 In this study, we made a number of adaptations to the original SynNotch system (Morsut et al., 2016)
84 in order to establish clonal modular SynNotch pluripotent cell lines (SyNPL). We characterised the
85 properties of this SyNPL system by monitoring interactions between EGFP-expressing sender cells and
86 mCherry-inducible receiver cells *in vitro*, then showed that this system can report interactions
87 between neighbouring cells *in vivo* in chimaeric mouse embryos, that it can be used for synthetic
88 patterning, and that its flexible and modular design can be exploited to conveniently manipulate cell-
89 cell interactions and drive contact-mediated synthetic cell fate engineering.

90

91 **RESULTS**

92 **Design of SyNPL ESCs**

93 We set out to adapt the SynNotch system, which was previously established through viral transduction
94 of immortalised mouse L929 fibroblasts and K562 erythroleukaemic cells (Morsut et al., 2016), for use
95 in mouse ESCs. In this system, sender cells are labelled with membrane-tethered extracellular EGFP
96 (Fig. 1B). Receiver cells constitutively express a SynNotch receptor composed of an anti-GFP nanobody
97 (LaG17) (Fridy et al., 2014), the mouse Notch1 minimal transmembrane core (Uniprot: Q01705,
98 residues 1427-1752), and a tetracycline transactivator (tTA) (Gossen and Bujard, 1992), and contain a
99 tetracycline response element (TRE) promoter capable of driving *mCherry* expression in response to
100 tTA binding (Fig. 1C). Interaction of EGFP on sender cells with the anti-GFP nanobody on receiver cells
101 leads to cleavage of the Notch1 core, releasing the tTA which can translocate to the nucleus, bind to
102 the TRE promoter and drive *mCherry* expression (Fig. 1D). In addition, we constitutively labelled
103 receiver cells with a tagBFP-3xNLS construct (Fig. 1C,D) to conveniently identify them by fluorescence
104 microscopy and flow cytometry even in the absence of a contact-dependent mCherry signal.

105 Our aims when adapting the SynNotch system were to generate ESC lines with low cell-cell variability,
106 robust and sustained transgene expression, and a modular design to allow convenient transgene

107 exchange. In order to avoid cell-cell variability we elected to generate clonal cell ESC lines with stable
108 genomic integration of the SynNotch system components, delivering transgenes by electroporation
109 rather than lentiviral transduction (Boggs et al., 1986; Charrier et al., 2011; Pfeifer et al., 2002;
110 Smithies et al., 1985). We sought to ensure uniform levels of transgene expression by screening clonal
111 lines and/or targeting transgenes to specific genomic locations, and by replacing the silencing-prone
112 SFFV retroviral promoter used by (Morsut et al., 2016) with CAG (Niwa et al., 1991) or mouse *Pgk1*
113 (McBurney et al., 1991) promoters, which have been extensively characterised in mouse ESCs (Chen
114 et al., 2011; Hong et al., 2007). Finally, we set out to introduce modularity to our system by generating
115 a "landing platform" master cell line to allow recombination-mediated cassette exchange (RMCE) of
116 transgenes of interest.

117 **Generation of extracellular membrane-tethered EGFP-expressing sender ESCs**

118 We first generated clonal sender cell lines expressing membrane-tethered extracellular EGFP. The CAG
119 and mouse *Pgk1* promoters are both silencing-resistant promoters commonly used to drive ubiquitous
120 transgene expression in ESCs (Herbst et al., 2012; Liew et al., 2007). We set out to determine which of
121 these promoters can generate viable sender cells with strong and uniform expression of membrane
122 EGFP. We also wished to explore whether EGFP molecules with HA and Myc protein tags can retain
123 "sender" function in pluripotent cells.

124 We electroporated mouse ESCs with four sender constructs, containing either CAG or mouse *Pgk1*
125 promoters driving expression of either untagged or HA- and Myc-tagged EGFP fused to a membrane-
126 tethering domain (Fig. 2A-D). We isolated and expanded 64 clonal lines derived from stable genomic
127 integration of the four constructs, and screened them by flow cytometry, analysing median EGFP
128 intensity (Fig. 2E,F), percentage of EGFP-positive cells (Fig. 2G,H) and EGFP distribution (Figs. S1, S2).
129 Both CAG and *Pgk1* promoters are capable of driving high uniform expression of EGFP, and, as
130 expected, there is considerable variability in EGFP expression between clonal lines.

131 We selected one untagged EGFP sender clone (CmGP1) and one HA- and Myc-tagged EGFP sender
132 clone (CHmGMP19), exhibiting high, uniform and similar levels EGFP expression (Fig. 2I) for further
133 analysis. For both clones, the pattern of EGFP expression appeared to be consistent with membrane
134 localisation, and, in the case of the HA- and Myc-tagged CHmGMP19 clone, the pattern of HA and Myc
135 expression appeared to coincide with that of EGFP (Fig. 2J).

136 **Generation of a safe harbour site landing pad master ESC line**

137 To facilitate convenient and repeated modification of the genome, we generated a clonal ESC line
138 carrying a "landing pad" targeted to the *Rosa26* locus, a safe harbour site in the mouse genome
139 (Friedrich and Soriano, 1991). This landing pad contains a splice acceptor, the *Neo* (G418/geneticin
140 resistance) gene, and a CAG promoter driving expression of *mKate2-3xNLS*, which encodes a red
141 fluorescent protein with no evident phenotypic effect in mouse embryos (Malaguti et al., 2013;
142 Shcherbo et al., 2009). This entire cassette is flanked by two *attP50* sites, which allows for ϕC31
143 integrase-mediated recombination with cassettes flanked by two *attB53* sites (Huang et al., 2009;
144 Tosti et al., 2018) (Fig. S3A). After confirming insertion at the correct genomic locus (Fig. S3B), we
145 verified that all cells express high and uniform levels of mKate2-3xNLS (Fig. S3C,D). We named this cell
146 line EM35.

147 **An "all-in-one" design fails to generate fully functional mCherry inducible receiver cells**

148 We first set out to investigate whether it would be possible to target all transcriptional units required
149 for receiver cell activity to the *Rosa26* landing pad in EM35 ESCs, and whether this would lead to the

150 generation of functional receiver ESCs. The design and characterisation of the resulting cell lines is
151 explained in detail in Supplementary Methods and Figs. S4-S9. Briefly, we found that mCherry could,
152 as expected, be induced by subpopulations of tagBFP-positive receiver cells in response to interaction
153 with EGFP-positive sender cells, but that this particular receiver cell design was hampered by variable
154 levels of tagBFP, variable inducibility of mCherry, and low levels of the SynNotch receptor. We
155 conclude that the SynNotch receptor construct and *TRE-mCherry* cassette can function as expected in
156 ESCs, but that further modifications to the design are required to obtain a reliable contact-reporting
157 system.

158 **A multi-step design produces fully functional mCherry-inducible receiver ESCs**

159 We hypothesised that two independent events may be affecting mCherry inducibility during our initial
160 attempts to generate "all-in-one-locus" receiver cells (Figs. S4-S9). Firstly, we speculated that *mCherry*
161 and *tagBFP* transgenes may have been lost from the genome due to mitotic recombination (Stern,
162 1936) or due to errors in replication at similar DNA sequences in close proximity (*Pgk1* promoters,
163 *bGHpA* signals). Secondly, we suspected that the expression levels of the SynNotch receptor were not
164 sufficient for efficient mCherry induction (Fig. S9).

165 We planned to circumvent the issue of potential loss of DNA by physically separating the three
166 transcriptional units through random genomic integration of the SynNotch receptor cassette and of
167 the *tagBFP-3xNLS* cassette, and by removing identical DNA sequences. To attempt to increase levels
168 of SynNotch receptor and to obtain uniform levels of tagBFP-3xNLS, we added an internal ribosome
169 entry site (IRES) followed by *Ble* (zeocin resistance gene) downstream of the SynNotch receptor
170 sequence, and an IRES followed by *Hph* (hygromycin B resistance gene) downstream of the *tagBFP-*
171 *3xNLS* sequence (Fig. 3A).

172 In order to generate these cells, we first randomly integrated the SynNotch receptor construct into
173 the genome of EM35 landing pad ESCs (Fig. S10A). We screened 87 clones for Myc expression, and
174 selected two clones (35SRZ9, 35SRZ86) with high, uniform Myc expression (Fig. S10B). The levels of
175 Myc in these clones were higher than those observed in receiver cells generated with an all-in-one
176 design (clones SNCB+4 and SNCB-6) and higher than those observed in Myc-tagged sender cells
177 (CHmGMP19) (Fig. S10C). We then randomly integrated the *tagBFP-3xNLS* transgene into the genome
178 of these two clones (Fig. S10D). We screened a total of 36 clones and selected one for each parental
179 line with high, uniform expression of tagBFP-3xNLS (PSNB-A clone 10, PSNB-B clone 3) (Fig. S10E,F).
180 We renamed these lines PSNB (Parental SynNotch tagBFP) clones A and B respectively.

181 Next, we performed RMCE at the *Rosa26* landing pad in PSNB cells to replace the *mKate2* transgene
182 with one of three constructs: the *TRE-mCherry* cassette present in the SCNB construct, a *tetO-mCherry*
183 cassette with more tTA binding sequences elements in the inducible promoter (to test whether this
184 led to improved mCherry induction), or an empty vector cassette to generate tagBFP-positive mKate2-
185 and mCherry-negative control cell lines (Fig. S11A). We verified that integration of the empty vector
186 cassette led to loss of mKate2 expression, and used these control cell lines to confirm that tagBFP
187 signal was able to unambiguously identify receiver cells (Figs. 3B,C, S11B).

188 We then set out to test whether the new receiver cell lines containing inducible mCherry cassettes
189 expressed mCherry in response to co-culture with sender cells. We screened 27 clones for tagBFP and
190 mCherry expression by culturing them in the presence or absence of sender cells for 24 hours (Fig.
191 S11C-G). We observed that all genetically identical clones behaved very similarly, suggesting we were
192 not experiencing silencing or loss of DNA. Clones containing the larger *tetO-mCherry* cassette
193 exhibited high levels of mCherry leakiness in the absence of sender cells. Co-culture with sender cells

194 led to significant mCherry induction, but the distributions in the presence and absence of sender cells
195 overlapped significantly (Fig. S11D,F,G). Clones containing the smaller *TRE-mCherry* cassette exhibited
196 mCherry leakiness in the absence of sender cells, however co-culture with sender cells led to an
197 increase in mCherry expression to levels which displayed minimal overlap with those seen in cells
198 cultured in the absence of sender cells (Fig. S11C,E,G). Leakiness in the absence of sender cells can be
199 reduced, but not abolished, by treatment of cells with the γ-secretase inhibitor DAPT (which inhibits
200 cleavage of the SynNotch receptor) or with doxycycline (which inhibits tTA-driven transcription) (Fig.
201 S12A,B).

202 We selected three clones with minimal leakiness and high inducibility for downstream analysis
203 (PSNBA-TRE1, PSNBB-TRE10, PSNBB-TRE9). We renamed these cells STC (for SynNotch-TRE-mCherry)
204 clones A1, B1 and B2 respectively. We verified that these receiver lines could induce mCherry following
205 cell-cell interaction with sender cells by co-culturing sender and receiver cells together for 24 hours.
206 We observed specific induction of mCherry by tagBFP-positive receiver cells in contact with EGFP-
207 positive sender cells (Fig. 3D). We used flow cytometry to confirm that mCherry is robustly induced in
208 the majority of tagBFP-positive receiver cells following co-culture with 9-fold excess of CmGP1 sender
209 cells at confluence (Fig 3B,C,E,F).

210 These observations suggest that physical separation of the three transcriptional units in the genome
211 of receiver cells, coupled to the use of internal ribosome entry sites and selectable markers within the
212 units, can lead to the generation of receiver ESC lines which exhibit clear and specific induction of
213 mCherry upon interaction with EGFP-expressing sender cells.

214 **Extracellular membrane-tethered EGFP is required for contact-mediated transgene induction in**
215 **receiver cells**

216 It would be useful to make use of existing GFP fluorescent reporter ESCs (for example, cell-state
217 reporters or signalling reporters) to act as sender cells, in order to test how particular cell states may
218 influence direct neighbours. However, many such cell lines make use of non-membrane-tethered GFP,
219 which is unlikely to interact with the anti-GFP nanobody on STC receiver cells. We therefore wished
220 to test whether membrane tethering of EGFP to the extracellular space was absolutely necessary for
221 effective neighbour-labelling.

222 We profiled mCherry levels in STC receiver cells by flow cytometry following 24 hours of co-culture
223 with "sender" cells carrying different transgenes (Fig. 3E-H). We cultured STC receiver cells alone (Fig.
224 3E), in the presence of CmGP1 sender cells (Fig. 3F), in the presence of a control cell line expressing
225 untagged intracellular EGFP (E14GIP1) (Fig. 3G), or in the presence of CmGP1 sender cells containing
226 an extra untagged intracellular EGFP transgene (CmGP1GH1) (Fig. 3H). We found that E14GIP1 cells,
227 which do not express membrane-tethered EGFP, did not induce mCherry above baseline levels in in
228 co-cultured STC receiver cells (Fig. 3E-G). Furthermore, we observed that mCherry is induced to similar
229 levels following co-culture with either CmGP1 or CmGP1GH1 sender cells (Fig. 3F,H), suggesting that
230 the additional untagged EGFP transgene in CmGP1GH1 cells does not interfere with mCherry induction
231 by the extracellular EGFP transgene. We conclude that cells containing intracellular GFP would not be
232 capable of functioning as sender cells unless supplemented with extracellular membrane tethered
233 EGFP.

234 **tagBFP-3xNLS lineage label allows identification of EGFP cross-labelled receiver cells**

235 In other cell types, a membrane-tethered anti-GFP nanobody can bind and internalise membrane-
236 tethered GFP on neighbouring cells (Tang et al., 2020). We find that this is also the case in ES cells (Fig.
237 S12B): punctuate EGFP signal is visible in mCherry-expressing activated receiver cells (Fig. S12C). It

238 could therefore be difficult to unambiguously separate of STC receiver cells from CmGP1 sender cells
239 by flow cytometry based on EGFP expression alone (Fig. S12D). This problem is overcome by making
240 use of the tagBFP-3xNLS lineage label in STC receiver cells. Furthermore, separation of sender and
241 receiver cells based on EGFP alone can be achieved if using CmGP1GH1 sender cells, which contain a
242 second EGFP transgene, leading to increased separation between sender cells and cross-labelled
243 receiver cells (Fig. S12F,G).

244 **Increasing sender:receiver cell ratios leads to increased transgene induction in receiver cells**

245 We next asked how differing sender:receiver cell ratios affect the efficiency of neighbour-labelling.
246 We co-cultured STC receiver cells with different proportions of sender cells for 24 hours (Fig. S13). We
247 observed that as few as 20% of sender cells were sufficient to induce mCherry in approximately half
248 of STC receiver cells, and that 90% sender cells could induce mCherry in over 90% of STC receiver cells
249 (Fig. S13A,B). mCherry fluorescence follows a bimodal distribution in receiver cells exposed to "non-
250 saturating" numbers of sender cells, and a unimodal distribution in receiver cells exposed to
251 "saturating" numbers of sender cells (Fig. S13C-H). This suggests that STC receiver cells which have
252 come into contact with sender cells can uniformly induce high levels of mCherry expression, as
253 observed by immunofluorescence when co-culturing cells at a 9:1 sender:receiver cell ratio (Fig. S13I-
254 K).

255 **HA- and Myc-tags on EGFP do not affect sender cell function**

256 An epitope tag fused to EGFP could be helpful for unequivocally identifying and isolating sender cells,
257 but carries the risk of interfering with sender function. Having generated sender cells with HA- and
258 Myc-tagged (CHmGMP19) and untagged (CmGP1) EGFP molecules, we sought to understand whether
259 tagged and untagged EGFP differed in their ability to induce transgene expression in receiver cells. We
260 therefore compared the ability of each sender line to induce mCherry expression in the previously
261 described experiment, where we cultured STC receiver cells with CmGP1 or CHmGMP19 sender cells
262 at varying sender:receiver cell ratios (Fig. S13). Both CmGP1 and CHmGMP19 sender cell lines can
263 drive mCherry induction to similar extents (Fig. S13A-H), suggesting that the LaG17 nanobody on the
264 SynNotch receptor can recognise both untagged and HA- and Myc-tagged EGFP, and that these tags
265 do not compromise sender function.

266 **Kinetics of contact-dependent transgene induction in receiver cells**

267 We next performed time-lapse microscopy. In order to capture a range of behaviours, we co-cultured
268 CmGP1GH1 sender cells with STC receiver cells at a 1:1 sender:receiver ratio at moderate density, and
269 filmed cells for 24 hours (Fig. 4A, Movie 1). mCherry first became visible 5-6 hours after initial sender-
270 receiver contact (Fig. 4A, yellow arrowheads). We observed STC receiver cells which did not make
271 contact with sender cells and remained mCherry-negative (Fig. 4A, magenta arrowheads), and an STC
272 receiver cell that made contact with a sender cell 2 hours before the cells were fixed at the 24-hour
273 timepoint for immunofluorescence, and which remained mCherry-negative (Fig. 4A, cyan
274 arrowheads).

275 We then quantified the kinetics of mCherry induction. We co-cultured 10% STC receiver cells with 90%
276 sender cells at high density in order to ensure interaction of almost every receiver cell with at least
277 one sender cell (Fig. 4B, Movie 2), and analysed mCherry expression in receiver cells by flow cytometry
278 over the course of 72 hours (Figs. 4C-E, S14A,B), and by live imaging over the course of 24 hours (Figs.
279 4B,F,G, S14C-H). mCherry is first induced at low levels at the 5-hour timepoint, and its expression
280 keeps increasing until the 48-hour timepoint (Figs. 4D-G, S14). We verified that mCherry signal

281 increases over time in receiver cells not only at the population level (Figs. 4D-F, S14A-E), but also within
282 individually tracked cells (Figs. 4G, S14F-H).

283

284 **Minimum time of contact required for transgene induction**

285 Relying on direct detection of mCherry (Fig 4C-G) is likely to overestimate the minimum duration of
286 cell contact required for mCherry induction because mCherry protein maturation will introduce a
287 time-lag between initiation of mCherry transcription and the detection of mCherry fluorescence. For
288 example, when analysing further time-lapse experiments (Fig. 5A, Movie 3), we noticed an example
289 of an STC receiver cell which remained in contact with a sender cell for 8 hours, lost contact for 12
290 hours following a cell division, but kept increasing its levels of mCherry in the meantime (Fig. 5A, white
291 arrowheads).

292 We designed an experimental strategy to overcome this problem. We co-cultured 10% STC receiver
293 cells with 90% CmGP1 sender cells for various time points between 0 and 24 hours, then added
294 doxycycline to the culture medium for a further 16 hours (Fig. 5B). Doxycycline prevents tTA from
295 binding to *TRE* sequences (Gossen and Bujard, 1992), hence we expect doxycycline administration to
296 halt *mCherry* transcription in receiver cells while still allowing time for mCherry protein to mature.
297 This means that any mCherry signal observed after doxycycline administration should be ascribable to
298 cell-contact-dependent transcription that took place during the initial period of co-culture in
299 doxycycline-free medium. In this experimental setting, we observed low but detectable induction of
300 mCherry when cells had experienced only 2 hours of doxycycline-free co-culture (Figs. 5C,D, S15).

301 These data collectively suggest that 2 hours of sender-receiver contact may be sufficient for induction
302 of low levels of mCherry, and that mCherry levels will keep increasing in receiver cells for a period of
303 time following the loss of sender-receiver contact. This neighbour-labelling system can therefore
304 identify receiver cells that have had relatively brief interactions with sender cells or which have
305 recently lost contact with sender cells.

306 **Kinetics of contact-dependent mCherry perdurance in receiver cells**

307 We next established how long mCherry signal persisted following loss of tTA-mediated *mCherry*
308 transcription. We co-cultured 10% STC receiver cells with 90% CmGP1GH1 cells for 24 hours, then
309 added doxycycline to the culture medium (to block the activity of tTA and halt mCherry transcription)
310 and filmed the cells over 48 hours (Fig. S16A,B, Movies 4,5). We observed little change in mCherry
311 fluorescence for the initial 8-12 hours, then a gradual decrease in signal until its extinguishment
312 around 38-40 hours after doxycycline addition (Fig. S16A,B). In order to quantify this process, we co-
313 cultured 10% STC receiver cells with 90% CmGP1 sender cells for 24 hours, then added doxycycline to
314 the culture medium and analysed mCherry fluorescence by flow cytometry at various timepoints (Fig.
315 S16C). No reduction of mCherry signal was observed for the initial 8 hours following doxycycline
316 administration, with median mCherry expression decreasing by approximately half by 16 hours, and
317 mCherry signal returning to background levels within 48 hours (Fig. S16D-F). Quantification of live
318 imaging data at hourly timepoints broadly confirmed these observations, with mCherry levels halving
319 after approximately 20-24 hours, and mCherry signal returning to background levels around 48 hours
320 (Fig. S16G).

321 Taken together, these results suggest that induction of mCherry occurs more rapidly than loss of
322 mCherry signal, presumably due to the high stability of this fluorescent protein, further confirming the
323 utility of this system for identifying recent as well as current cell-cell interactions.

324 **The SyNPL SynNotch cell-cell interaction reporter is functional in early mouse embryos**

325 Having comprehensively characterised the SynNotch system in clonal mouse ESC lines, we set out to
326 test whether the system could also function *in vivo* in early mouse embryos. We aggregated wild-type
327 morulae with CmGP1GH1 sender cells and/or STC receiver cells, and cultured these to the blastocyst
328 stage (Fig. 6). As expected, all chimaeric blastocysts (80/80) containing both sender and STC receiver
329 cells induced expression of mCherry, whereas no wild-type blastocysts nor blastocysts containing only
330 sender cells displayed mCherry expression (Fig. 6A,B). 18 out of 19 chimaeras containing STC receiver
331 cells alone did not express readily detectable levels of mCherry (Fig. 6B), in line with the low proportion
332 of mCherry-high cells observed *in vitro* in STC receiver cells cultured alone. Treatment of chimaeric
333 embryos with the γ-secretase inhibitor DAPT suppressed mCherry induction, and withdrawal of DAPT
334 allowed mCherry upregulation (Fig. S17), confirming that SynNotch receptor cleavage is required for
335 mCherry induction.

336 All three STC clonal lines reliably induced mCherry within chimaeric embryos that also contained
337 CmGP1GH1 sender cells (Fig. 5B, Fig. S18A), with mCherry generally appearing within 20h of
338 aggregation (Movie 6). As expected, some receiver cells remain unlabelled when given limited access
339 to sender cells within chimeric blastocysts (aggregations performed with eight receiver cells and only
340 one sender cell: Fig. S18B), in keeping with the contact-dependent nature of SynNotch activation.
341 Post-implantation chimaeras containing both sender and receiver cells displayed mCherry induction
342 throughout the body axis (Fig. S18C). These results suggest that the SyNPL neighbour-labelling system
343 is functional, efficient and reliable *in vivo*.

344 **Spatial confinement of sender and receiver cells leads to synthetic patterning**

345 SynNotch technology has been successfully employed to generate synthetic patterns. Strategies to
346 achieve this include co-culturing cells in a low sender:receiver cell ratio in order to create 2-
347 dimensional activated receiver cell rings surrounding a clone of sender cells (Morsut et al., 2016),
348 creating self-organising cell aggregates through contact-mediated induction of adhesion molecules
349 (Toda et al., 2018), and recreating morphogen gradients through the use of anchor proteins to capture
350 diffusible receiver cell-activating signal (Toda et al., 2020).

351 We set out to test whether our clonal ESC lines could be used to generate a synthetic pattern: a stripe
352 of transgene expression at the region of contact between sender and receiver cells. To this end, we
353 plated CmGP1 sender and STC receiver cells in separate chambers of a removable multi-chamber cell
354 culture insert and allowed them to reach confluence. We then removed the insert, allowing cells to
355 grow in the space between chambers, make contact and induce transgene expression in receiver cells
356 (Fig. 7A; a detailed description of stripe generation and characterisation can be found in
357 Supplementary Methods and in Fig. S19). We assessed expression of mCherry 24 hours after initial
358 sender:receiver contact, and observed a distinct stripe of mCherry expression at the sender:receiver
359 border (Fig. 7B). This result suggest that SynNotch technology can be successfully employed in mouse
360 ESCs to generate synthetic patterns of gene expression.

361 **Harnessing modularity of SyNPL SynNotch ESCs to synthetically alter cell fate**

362 One advantage of introducing modularity to our SyNPL SynNotch system design is that we can
363 generate clonal receiver cell lines with inducible expression of any gene of interest. Having
364 characterised the system in mCherry-inducible STC receiver cells, we wished to test whether we could
365 alter receiver cell fate following interaction with sender cells by generating Neurog1-inducible receiver
366 cells.

367 The transcription factor Neurog1 (Neurogenin 1) is necessary for neural development in mice, where
368 it drives neuronal differentiation of progenitor cells (Cau et al., 2002; Ma et al., 1998; Yuan and Hassan,
369 2014). Ectopic expression of Neurog1 has been shown to lead to neuronal differentiation both in
370 ectoderm and, surprisingly, in mesoderm (Cai et al., 2000; Ma et al., 1996; Perez et al., 1999). This
371 ability of Neurog1 to induce differentiation in non-permissive conditions was exploited to drive
372 neuronal differentiation of mouse ESCs in pluripotent culture conditions (Velkey and O'Shea, 2013).
373 We therefore set out to ask whether contact-mediated induction of a *Neurog1* transgene could induce
374 neuronal differentiation specifically in receiver cells that come into contact with EGFP-expressing
375 sender cells.

376 Firstly, we generated STN (SynNotch TRE-Neurog1) receiver cells by performing RMCE at the *Rosa26*
377 landing pad in PSNB cell lines to replace the *mKate2-3xNLS* transgene with a *TRE-3xFlag-Neurog1*
378 cassette (Figs. 7C, S20A). We then tested whether we could drive contact-mediated induction of the
379 *Neurog1* transgene by co-culturing STN receiver cells with CmGP1 senders cells for 48 hours, the
380 timepoint at which we observed maximum mCherry induction in STC receiver cells (Figs. 4C,D, S14A,B).
381 We confirmed this resulted in robust induction of 3xFlag-Neurog1 in STN receiver cells compared to
382 STN receiver cells cultured alone (Fig. S20B), which suggests that PSNB landing pad cell lines can be
383 used to generate receiver cells harbouring inducible transgenes other than mCherry.

384 We then set out to test whether we could induce contact-mediated neuronal differentiation of
385 receiver cells in pluripotent culture conditions, and whether we could engineer differentiation to occur
386 in a synthetic pattern. To this end, we repeated the synthetic stripe patterning experiment described
387 above (Fig. 7A,B), using STN receiver cells in place of STC receiver cells. We assessed the expression of
388 the neuronal marker Tubb3 96 hours after initial sender:receiver contact, and observed evident
389 induction of Tubb3 and acquisition of neuronal morphology by STN receiver cells at the
390 sender:receiver border (Fig. 7D). We verified that E14GIP1 cytoplasmic EGFP control cells were unable
391 to induce neuronal differentiation at the border with STN receiver cells (Fig. S21A). We observed that
392 Neurog1 is induced shortly after initial sender:receiver cell contact (Fig. S21B), and that Tubb3
393 induction first occurs 48 hours after initial interaction between sender and STN receiver cells (Fig.
394 S21C).

395 We conclude that the interaction between EGFP-expressing sender cells and STN receiver cells can
396 lead to contact-mediated *Neurog1* induction and neuronal differentiation of receiver cells in non-
397 permissive culture conditions. This demonstrates that the SyNPL system can be readily used to
398 generate clonal ESC lines for contact-mediated induction of transgenes of interest, and that these cell
399 lines can in turn be used to manipulate cell-cell interactions in order to program synthetic cell fate
400 decisions in response to contact with a particular cell population at desired locations in space.

401

402 **DISCUSSION**

403 Engineering SynNotch machinery (Morsut et al., 2016) into pluripotent cells opens up many
404 opportunities for understanding how direct cell-cell interactions between neighbouring cells can
405 control differentiation decisions, mediate cell competition (Sancho et al., 2013) and orchestrate
406 morphogenesis (Gorfinkiel and Martinez Arias, 2021) as cells differentiate in 2D or 3D culture. Mouse
407 ES cells have the unique ability to contribute to chimaeric embryos, meaning that appropriately
408 engineered cell lines can also be used to understand and control cell-cell interactions during early
409 embryonic development. There are however particular challenges associated with engineering
410 existing SynNotch technologies into pluripotent cells. Here we describe how we overcame these

411 challenges to generate the SyNPL system: a set of clonal SynNotch "sender" and "receiver" mouse ES
412 cells engineered with optimised and modular SynNotch technology. We demonstrate the utility of the
413 SyNPL system for monitoring cell-cell interactions both in culture and in early mouse embryos, and
414 show that we can use this system to engineer contact-dependent cell fate decisions at the boundary
415 between two populations of pluripotent cells.

416 **Properties of sender cells**

417 We generated sender cell lines expressing high and uniform levels of extracellular membrane-tethered
418 EGFP. This transgenic construct was previously used for SynNotch sender cells (Morsut et al., 2016;
419 Sgodda et al., 2020), and comprises EGFP fused to an N-terminal mouse IgGK signal sequence and a C-
420 terminal human PDGFRB transmembrane domain. The addition of HA and Myc tags at the N- and C-
421 termini of EGFP did not affect the ability of sender cells to induce mCherry expression in STC receiver
422 cells (Fig. S13), suggesting that the antigenic region of EGFP recognised by the LaG17 anti-GFP
423 nanobody component of the SynNotch receptor is not masked by the HA and Myc protein tags.
424 Furthermore, the LaG17 anti-GFP nanobody can also bind to *Aequorea victoria* YFP, CFP and BFP, and
425 *Aequorea macrodactyla* CFP (Fridy et al., 2014), raising the interesting possibility that transgene
426 induction in our receiver cells could be induced by sender cells expressing different membrane-
427 tethered fluorophores.

428 Mouse ESCs and mouse lines labelled with lipid anchor-tethered GFP constructs have previously been
429 described (Kondoh et al., 1999; Nowotschin et al., 2009; Rhee et al., 2006; Shioi et al., 2011). It would
430 be interesting to test if these lines could function as SynNotch sender cells; this would require
431 extracellular GFP localisation and generation of sufficient tensile force upon receptor interaction
432 (Morsut et al., 2016). GPI anchors GFP to the outer leaflet of the plasma membrane (Rhee et al., 2006;
433 Sevcsik et al., 2015); GFP-GPI-labelled cells should therefore be capable of acting as sender cells. This
434 does indeed appear to be the case in *Drosophila* (He et al., 2017).

435 **"All-in-one" locus receiver cells display suboptimal functionality**

436 Our initial attempts at generating "all-in-one" *Rosa26*-targeted receiver cells (termed SNCB+ and
437 SNCB- cells) were unsuccessful. The large variation in tagBFP expression and low proportion of
438 mCherry-inducible ESCs we saw within all of our purportedly genetically identical clonal lines suggests
439 that either widespread transgene silencing or loss of DNA occurred at the *Rosa26* safe harbour locus
440 in pluripotent cells. Furthermore, the observation that rederivation of clonal lines following
441 fluorescence-activated cell sorting of single SNCB+ and SNCB- cells led to re-establishment of the initial
442 heterogeneous distributions of fluorophore expression (Figs. S7, S8) suggests that the all-in-one design
443 is not optimal for use in pluripotent cells. We were able to overcome these problems by switching to
444 a random-integration strategy, but it is possible that inclusion of IRES-antibiotic resistance cassettes
445 and/or insulator sequences may provide an alternative route towards generating a reliable system
446 without sacrificing the all-in-one-locus approach.

447 **Landing pad ESCs provide system modularity**

448 Targeting of a landing pad to the *Rosa26* safe harbour locus has been previously characterised as an
449 efficient strategy for the rapid generation of multiple cell lines through RMCE (Seibler et al., 2005;
450 Tchorz et al., 2012; Tosti et al., 2018). We found this to be true for our cell lines harbouring a *Rosa26-*
451 *attP50-Neo-mKate2-attP50* landing pad, which we used to generate several different cell lines with
452 ease. The advantage of such a system is the ability to target different transgenes to the same genomic
453 locus in the same parental cell line. Our parental PSNB lines harbouring the *Rosa26* landing pad
454 allowed us to initially test the functionality of SynNotch in ESCs with an inducible *mCherry* transgene

455 in STC receiver cells, prior to generating genetically equivalent STN receiver cells with a *Neurog1*
456 transgene in place of *mCherry*. This modular design therefore makes it possible to readily switch
457 between using SyNPL for monitoring and profiling the consequences of defined cell-cell interactions
458 (based on contact-dependent mCherry expression) and using SyNPL for engineering contact-
459 dependent cell behaviours (based on contact-dependent expression of any cell behaviour-
460 determinant).

461 **Describing the properties of the SyNPL system**

462 We characterised various aspects of the SyNPL system that will help inform the experimental design
463 for users of these cells.

464 Previous studies have co-cultured senders and receiver cells at different ratios (ranging from 1:50 to
465 5:1), and for varying times (ranging from 10 minutes to several days) (Cho et al., 2018; Choe et al.,
466 2021; He et al., 2017; Huang et al., 2020; Luo et al., 2019; Matsunaga et al., 2020; Morsut et al., 2016;
467 Roybal et al., 2016; Sgodda et al., 2020; Srivastava et al., 2019; Toda et al., 2018; Toda et al., 2020;
468 Wang et al., 2021; Yang et al., 2020). We analysed transgene induction in STC receiver cells at 11
469 different sender:receiver cell ratios (ranging from 1:19 to 9:1), and observed that higher proportions
470 of sender cells in culture result in a higher proportion of receiver cells inducing mCherry. This is in line
471 with the results obtained by (Sgodda et al., 2020) when comparing three different sender:receiver cell
472 ratios, and with the observations of (Morsut et al., 2016), who exposed receiver cells to varying
473 concentrations of sender ligand. By finely varying the concentrations of sender ligand, Lim and
474 colleagues described the transgene induction response as sigmoidal (Morsut et al., 2016), which was
475 not evident in our data. It is however possible that by testing lower sender:receiver cell ratios this
476 might hold true in our SynNotch system too.

477 When analysing transgene expression within single samples, we found that mCherry distribution
478 follows a bimodal on/off response, indicative of the presence of receiver cells which do not interact
479 with sender cells at low sender:receiver cell ratios. This bimodal pattern of transgene induction is also
480 evident in data from Cantz and colleagues (Sgodda et al., 2020). The ability of individual sender cells
481 to induce mCherry induction in STC receiver cells (as seen in Movies 1 and 3) implies that this system
482 can be effectively employed to study the effect of interactions between receiver cells and individual
483 and/or rare sender cells in relevant model systems.

484 We performed a high-resolution study of the kinetics of mCherry induction and downregulation in STC
485 receiver cells. We observed low levels of mCherry induction in STC receiver cells following 2 hours of
486 co-culture with sender cells, provided we allowed time for subsequent protein maturation, and
487 observed maximum mCherry induction following 48 hours of co-culture. Previous studies making use
488 of lentiviral-delivered transgenes suggest that 10 minutes may be sufficient for transgene activation
489 in HEK293 receiver cells, and that 1 hour may be sufficient for transgene induction in L929 receiver
490 cells, as long as protein maturation time is allowed (Morsut et al., 2016; Sgodda et al., 2020). This is
491 significantly faster than what we observed in this study, and may be ascribable to lentiviral
492 transduction leading to higher levels of SynNotch receptor and/or integration of multiple transgene
493 copies compared to our clonal mouse ESC lines.

494 In our system, mCherry downregulation did not commence for at least 8 hours following simulated
495 loss of sender:receiver cell contact, with full loss of signal occurring after more than 40 hours. This is
496 in line with previous observations in L929 receiver cells, where inducible GFP transgene expression
497 was lost between 24 and 50 hours after sender cells were removed from culture (Morsut et al., 2016).

498 The kinetics of mCherry induction and downregulation suggest that this SynNotch system is suited for
499 the study of cell-cell interactions with a temporal range of hours rather than minutes, and that
500 "memory" of such interactions will persist for a few days. mCherry signal intensity will be influenced
501 not only by the duration of contact but also, where cells have moved apart, by the time elapsed since
502 last contact: this may complicate interpretation of data from this system for some applications. Should
503 this persistence of mCherry signal prove inconvenient for the study of particular processes, the PSNB
504 landing pad parental cell lines can be used to readily generate cell interaction reporter receiver cells
505 harbouring destabilised inducible transgenes with short half-lives.

506 **Exploring the roles of cell-cell interactions *in vivo* and *in vitro***

507 We demonstrated that our clonal mouse ESC lines can be used *in vivo* in chimaeric embryos. The ability
508 to conveniently switch between *in vitro* and *in vivo* experimentation was a key reason for us to
509 establish SynNotch technology in mouse ESCs. Both the receiver lines we generated and the parental
510 PSNB landing pad cell lines offer the power and flexibility to address questions we have so far been
511 unable to answer in *in vitro* and *in vivo* settings. For example, the system could be employed in cell
512 competition studies: STC receiver cells could be used to identify and isolate the direct neighbours of
513 EGFP-tagged "loser" cells, and profiled to study what changes are induced upon interaction with loser
514 cells in order to bring about their elimination. Receiver cells could also be engineered to express
515 candidate fitness-altering transgenes in response to interaction with EGFP-tagged wild-type sender
516 cells, as successfully demonstrated in *Drosophila* by (He et al., 2017).

517 The establishment of this system in mouse ESCs also allows to monitor and manipulate the effects of
518 cell-cell interactions in specific cell types obtained through directed differentiation. We also
519 demonstrated that our cell lines can be used to generate synthetic patterns of gene expression,
520 resulting in spatially-defined programming of cell fate. The combination of directed differentiation of
521 ESCs, spatial confinement of sender and receiver cells, and contact-mediated cell fate engineering
522 provides many possibilities for the study of cell-cell interactions in any developmental process of
523 interest.

524 **Concluding remarks**

525 Cell-cell interactions are a shared feature of the development of all multicellular organisms. Whilst the
526 particulars of these interactions vary greatly amongst eukaryotic supergroups, it is clear that they play
527 an essential role in development (Armingol et al., 2021). The Synthetic Biology field has recently
528 developed several applications to monitor cell communication, such as SynNotch (Morsut et al., 2016)
529 and derivative systems (Zhu et al., 2021), direct transfer of fluorophores to neighbouring cells
530 (Ombrato et al., 2019; Tang et al., 2020), reconstitution of a fluorophore following interaction
531 between different cell types carrying non-fluorescent fluorophore fragments (Kinoshita et al., 2020).
532 We have here demonstrated how SynNotch technology can be used to monitor and manipulate cell-
533 cell interactions in mouse ESCs and in mouse embryos. We hope that the SyNPL system will prove a
534 useful and adaptable tool for the mouse Stem Cell and Developmental Biology community.

535

536 **MATERIALS AND METHODS**

537 **Reagents**

REAGENT	SOURCE	IDENTIFIER	CONCENTRATION
Antibodies and nuclear counterstain			

Mouse monoclonal anti-Flag	Sigma-Aldrich	Cat# F3165; RRID: AB_259529	1:1000
Chicken polyclonal anti-GFP	Abcam	Cat# ab13970; RRID: AB_300798	1:1000
Goat polyclonal anti-Myc	Abcam	Cat# ab9132; RRID: AB_307033	1:1000
Mouse monoclonal anti-Myc AlexaFluor 488 conjugate	Santa Cruz	Cat# sc-40 AF488; RRID: AB_2892598	1:200
Rabbit polyclonal anti-LaminB1	Abcam	Cat#ab16048; RRID: AB_443298	1:1000
Rat monoclonal anti-mCherry	Invitrogen	Cat# M11217; RRID: AB_2536611	1:1000
Mouse monoclonal anti-Nup107 (NPC)	Abcam	Cat# ab24609; RRID: AB_448181	1:1000
Rabbit polyclonal anti-tRFP (tagBFP)	Evrogen	Cat# AB233; RRID: AB_2571743	1:1000
Mouse monoclonal anti-Tubb3	Biolegend	Cat# 801201; RRID: AB_2313773	1:1000
DRAQ7	Abcam	Cat# ab109202	1µM (IF); 300nM (flow cytometry)
DAPI	Biotium	Cat# 40043	1µM
Chemicals and solutions			
2-Mercaptoethanol	Gibco	Cat# 31350010	100nM
Accutase	Sigma-Aldrich	A6964	
Benzyl alcohol	Alfa Aesar	Cat# 100-51-6	
Benzyl benzoate	Sigma	Cat# B9550	
Chorulon (hCG)	Intervet	Cat# CH-475-1	100 IU/ml
DAPT	Abcam	Cat# ab120633	100µM
DMEM, high glucose, no glutamine, no phenol red	Gibco	Cat# 31053028	
Donkey serum	Sigma-Aldrich	Cat# D9663	3% v/v
Doxycycline hyclate	Sigma-Aldrich	Cat# D9891	1µg/ml
Dulbecco's phosphate buffered saline (PBS)	Sigma-Aldrich	Cat# D8537	
Fibronectin from bovine plasma solution	Sigma-Aldrich	Cat# F1141	
Foetal calf serum	Life Technologies	Cat# 10270106	10% v/v
Formaldehyde 37-41%	Fisher Scientific	Cat# F/1501/PB08	4% w/v
Gelatin	Sigma-Aldrich	Cat# G1890	0.1% w/v

Geneticin (G418)	Gibco	Cat# 11811031	200µg/ml
Glasgow Minimum Essential Medium	Sigma-Aldrich	Cat# G5154	
Hygromycin B	Gibco	Cat# 10687010	200µg/ml
L-Glutamine	Thermo Scientific	Cat# 25030024	2mM
Lipofectamine 3000 transfection reagent	Life Technologies	Cat# L3000008	
M2 medium	Sigma-Aldrich	Cat# M7167	
MEM Non-essential amino acids solution (100X)	Gibco	Cat# 11140050	1X
Penicillin/streptomycin	Gibco	Cat# 15140122	100 U/ml
PMSG	ProSpec	Cat# HOR-272	100 IU/ml
Prolong Gold Antifade Mountant	Thermo Fisher	Cat# P36930	
Puromycin dihydrochloride	Sigma-Aldrich	Cat# P8833	2µg/ml
Sodium pyruvate	Gibco	Cat# 11360039	1 mM
Triton X-100	Sigma-Aldrich	Cat# X100	0.1% v/v
Trypsin EDTA 0.25%	Gibco	Cat# 25200072	0.05% w/v
Tyrode's solution, acidic	Sigma-Aldrich	Cat# T1788	
Zeocin	Gibco	Cat# R25001	100µg/ml
Cell culture substrates and inserts			
3 well silicone culture insert	Ibidi	Cat# 80369	
µ-Slide 8 Well	Ibidi	Cat# 80826	
µ-Slide 4 Well	Ibidi	Cat# 80426	
µ-Plate 96 Well Black	Ibidi	Cat# 89626	
µ-Slide Angiogenesis, uncoated	Ibidi	Cat# 81501	
Glass coverslip, 24mm diameter	VWR	Cat# 631-1583	
Plastic flasks and plates for routine cell culture	Corning	Various	
DNA constructs			
pHR_EGFPligand	(Morsut et al., 2016)	Addgene 79129	
pHR_SFFV_LaG17_synNotch_TetRVP64	(Morsut et al., 2016)	Addgene 79128	
pDisplay-EGFP-TM	(Han et al., 2004)		
pHR_TRE-mCherry-PGK-tagBFP-WPRE	Elise Cachat, University of Edinburgh		
CAG-ϕC31 integrase	(Monetti et al., 2011)	Similar plasmid available: Addgene 62658	
pRosa26-DEST-1lox	(Tosti et al., 2018)		
pENTR-2xAttP50	(Tosti et al., 2018)		
pENTR-2xAttB53	(Tosti et al., 2018)		
pPyCAG-EGFP-TM-IRES-Pac	This study	Addgene 183603	
pPyPGK-EGFP-TM-IRES-Pac	This study	Addgene 183604	
pPyCAG-HA-EGFP-Myc-TM-IRES-Pac	This study	Addgene 183605	

pPyPGK-HA-EGFP-Myc-TM-IRES-Pac	This study	Addgene 183606	
pPyPGK-Myc-LaG17-Notch1TM-tTA-IRES-Ble	This study	Addgene 183607	
pPyCAG-tagBFP-3xNLS-IRES-Hph	This study	Addgene 183608	
pmROSA26-attP50-Neo-mKate2-3xNLS-attP50	This study	Addgene 183609	
attB53-Pac-attB53	This study	Addgene 183610	
attB53-Pac-TRE-mCherry-attB53	This study	Addgene 183611	
attB53-Pac-tetO-mCherry-attB53	This study	Addgene 183612	
attB53-Pac-TRE-3xFlag-Neurog1-attB53	This study	Addgene 183613	
attB53_SNCB+_attB53	This study	Addgene 183614	
attB53_SNCB-_attB53	This study	Addgene 183615	
Cell lines			
E14Ju09 mouse ESCs (129/Ola, male)	(Hamilton and Brickman, 2014)		
CmGP1 sender mouse ESCs (129/Ola, male)	This study		
CHmGMP19 sender mouse ESCs (129/Ola, male)	This study		
CmGP1GH1 sender mouse ESCs (129/Ola, male)	This study		
E14GIP1 mouse ESCs (129/Ola, male)	This study		
EM35 mouse ESCs (129/Ola, male)	This study		
SNCB+ receiver mouse ESCs (129/Ola, male)	This study		
SNCB- receiver mouse ESCs (129/Ola, male)	This study		
35SRZ mouse ESCs (129/Ola, male)	This study		
PSNB mouse ESCs (129/Ola, male)			
PSNB-E mouse ESCs (129/Ola, male)	This study		
PSNB-tetO receiver mouse ESCs (129/Ola, male)	This study		
STC receiver mouse ESCs (129/Ola, male)	This study		
STN receiver mouse ESCs (129/Ola, male)	This study		

538

539 **Animal care and use**

540 Animal experiments were performed under the UK Home Office project license PEEC9E359, approved
541 by the Animal Welfare and Ethical Review Panel of the University of Edinburgh and within the
542 conditions of the Animals (Scientific Procedures) Act 1986.

543 **Chimaera generation**

544 C57BL/6 female mice (Charles River) were superovulated (100 IU/ml PMSG and 100 IU/ml hCG
545 intraperitoneal injections 48 hours apart) and crossed with wild-type stud male mice. Pregnant mice
546 were culled at embryonic day 2.5 (E2.5) by cervical dislocation, ovaries with oviducts were dissected
547 and collected in pre-warmed M2 medium. Oviducts were flushed using PBS and a 20-gauge needle

548 attached to a 1ml syringe and filled with PB1 (Whittingham, 1974). E2.5 embryos were collected and
549 washed in PB1, their zona pellucida was removed using acidic Tyrode's solution, and they were
550 transferred to a plate with incisions where two clumps of approximately 8 sender and 8 receiver cells
551 were added to each embryo. Embryos were then incubated at 37°C in 5% CO_2 for 48 hours prior to
552 fixation, or for 24 hours prior to transfer to pseudopregnant females for the generation of post-
553 implantation chimaeras. For DAPT treatment experiments, DAPT was equilibrated for several hours at
554 37°C prior to addition to embryos in order to avoid precipitation. Embryos subject to DAPT withdrawal
555 were washed twice before being placed in DAPT-free medium. The sex of embryos used in this study
556 was not determined.

557 **Mouse ESC culture**

558 Mouse embryonic stem cells were routinely maintained on gelatinised culture vessels (Corning) at
559 37°C and 5% CO_2 in Glasgow Minimum Essential Medium (GMEM) supplemented with 10% foetal calf
560 serum (FCS), 100U/ml LIF (produced in-house), 100nM 2-mercaptoethanol, 1X non-essential amino
561 acids, 2mM L-Glutamine), 1mM Sodium Pyruvate (medium referred to as "ES cell culture medium" or
562 "LIF+FCS"). The medium was supplemented with 200µg/ml G418, 2µg/ml puromycin, 200µg/ml
563 hygromycin B and/or 100µg/ml zeocin as appropriate.
564 For live imaging, GMEM was replaced with phenol red-free Dulbecco's Modified Eagle Medium
565 (DMEM), with all other components of the culture medium used at identical concentrations.

566 **DNA constructs**

567 pHR_SFFV_LaG17_synNotch_TetRVP64 (Addgene plasmid #79128) (Morsut et al., 2016) and
568 pHR_EGFPligand (Addgene plasmid #79129) (Morsut et al., 2016) were kind gifts from Dr Wendell Lim
569 (UCSF) and Dr Leonardo Morsut (USC). pDisplay-GFP-TM (Han et al., 2004) was a kind gift of Dr Luis
570 Ángel Fernández (CNB-CSIC). CAG-ϕC31 integrase (Monetti et al., 2011) was a kind gift of Dr Andras
571 Nagy (Lunenfeld-Tanenbaum Research Institute). pHR_TRE-mCherry-PGK-tagBFP-WPRE was a kind
572 gift of Dr Elise Cachat (The University of Edinburgh). pRosa26-DEST-1lox, pENTR-2xAttP50 and pENTR-
573 2xAttB53 (Tosti et al., 2018) constructs were kind gifts of Dr Keisuke Kaji (The University of Edinburgh).

574 Untagged transmembrane EGFP constructs were generated by digesting pHR_EGFPligand with
575 XhoI+NotI, and ligating the *IgGK signal-EGFP-PDGFRB TMD* cassette into XhoI+NotI-digested *pPyCAG-*
576 *IRES-Pac* (Malaguti et al., 2019) or *pPyPGK-IRES-Pac* (Rao et al., 2020) vector backbones. HA- and Myc-
577 tagged EGFP constructs were generated by PCR-amplifying an *IgGK signal-HA-EGFP-Myc-PDGFRB TMD*
578 cassette flanked by PspXI and NotI sites from pDisplay-GFP-TM, digesting the amplicon with
579 PspXI+NotI, and ligating the insert into XhoI+NotI-digested *pPyCAG-IRES-Pac* or *pPyPGK-IRES-Pac*
580 vector backbones.

581 The *pPyPGK-CD8a signal-Myc-LaG17-Notch1 minimal transmembrane core-tTA-IRES-Ble* SynNotch
582 receptor construct was generated by PCR-amplifying a *CD8a signal-Myc-LaG17-Notch1 minimal*
583 *transmembrane core-tTA* cassette flanked by XhoI and Bsu36I sites from
584 pHR_SFFV_LaG17_synNotch_TetRVP64, digesting the amplicon with XhoI+Bsu36I, and ligating the
585 insert into a XhoI+Bsu36I-digested *pPyPGK-IRES-Ble* vector backbone. The mouse Notch1 minimal
586 transmembrane core consists of residues 1427-1752 (Uniprot: Q01705).

587 The *pPyCAG-tagBFP-3xNLS-IRES-Hph* construct was generated by PCR-amplifying a *tagBFP* cassette
588 flanked by XhoI and KasI sites from pHR_TRE-mCherry-PGK-tagBFP-WPRE, digesting the amplicon with
589 XhoI+KasI, and ligating the insert into a XhoI+NotI-digested *pPyCAG-IRES-Hph* backbone (Malaguti et
590 al., 2019) alongside oligonucleotides annealed to generate a *3xNLS* fragment with KasI and NotI
591 overhangs (Malaguti et al., 2013).

592 The *Rosa26* landing pad targeting vector was generated by Gateway Cloning (Invitrogen) of an *attL1-*
593 *attP50-Neo-SV40pA-(CAG-mKate2-3xNLS-bGHpA)-attP50-attL2* cassette into the pRosa26-DEST-1lox
594 targeting vector. Its final structure is as follows: *Rosa26 5'HA-splice acceptor-loxP-attP50-Neo-*
595 *SV40pA-(CAG-mKate2-3xNLS-bGHpA)-attP50-Rosa26 3'HA-PGK-DTA-bGHpA*. Sequence in brackets is
596 on -strand.

597 An *attB53-Pac-attB53* "empty vector" construct for RMCE at the *Rosa26* locus was generated by
598 adding a *Pac-bGHpA* cassette followed by an EcoRV restriction site to pENTR-2xAttB53 by Gibson
599 assembly.
600 The attB53-TRE-mCherry-attB53 RMCE construct used to generated STC receiver cells from PSNB
601 landing pad lines was generated by PCR-amplifying a *TRE-mCherry-SV40pA* cassette flanked by EcoRV-
602 AscI and EcoRV-BamHI sites from pHR_TRE-mCherry-PGK-tagBFP-WPRE, digesting the amplicon with
603 EcoRV, ligating the insert into EcoRV-digested *attB53-Pac-attB53* backbone, and screening for
604 insertion on the -strand. The attB53-tetO-mCherry-attB53 RMCE construct used to generate PSNB-
605 tetO cells from PNSB landing pad lines was generated by PCR-amplifying a *tetO-mCherry-rBGpA*
606 cassette flanked by MluI and BamHI sites, digesting the amplicon with MluI+BamHI and ligating the
607 insert into AscI+BamHI-digested *attB53-Pac-TRE-mCherry-attB53*.
608 The attB53-TRE-3xFlag-Neurog1-attB53 RMCE construct used to generate STN receiver cells from
609 PSNB landing pad lines was generated by PCR-amplifying a *3xFlag-Neurog1* cassette flanked by NdeI
610 and MfeI sites from wild-type mouse cDNA, digesting the amplicon with NdeI+MfeI and ligating the
611 insert into NdeI+MfeI-digested *attB53-Pac-TRE-mCherry-attB53* backbone (in which *mCherry* is
612 flanked by NfeI and MfeI sites).

613 attB53_SNCB+_attB53 and attB53_SNCB_attB53 constructs were generated in two steps. First, the
614 base *attB53-Pac-bGHpA-attB53* RMCE construct was linearised with EcoRV, and ligated with a HincII-
615 *PGK-CD8a signal-Myc-LaG17-Notch1 minimal transmembrane core-tTA*-HindIII fragment (digested
616 from the SynNotch receptor construct described above) and a HindIII-*bGHpA*-EcoRV fragment, and
617 clones were screened for insertion of the SynNotch receptor on the +strand. Next, the resulting
618 construct was linearised with EcoRV, and ligated with an EcoRV-*TRE-mCherry-SV40pA-PGK-tagBFP-*
619 PacI fragment (digested from pHR_TRE-mCherry-PGK-tagBFP-WPRE) and a PacI-*bGHpA*-EcoRV
620 fragment. Correct assembly on the + and - strands generated the attB53_SNCB+_attB53and
621 attB53_SNCB-_attB53 constructs respectively.

622 Abbreviations: TMD: transmembrane domain; IRES: internal ribosome entry site; 5'/3' HA: 5'/3'
623 homology arm; SV40pA: SV40 polyadenylation signal sequence; bGHpA: bovine growth hormone
624 polyadenylation signal sequence; rBGpA: rabbit beta-globin polyadenylation signal sequence; NLS:
625 nuclear localisation signal; PGK: mouse *Pgk1* promoter; Pac: puromycin N-acetyltransferase; Hph:
626 hygromycin B phosphotransferase; Ble: bleomycin resistance gene (confers zeocin resistance); tTA:
627 tetracycline transactivator.

628 Plasmids that we generated for this study will be made available on Addgene.

629 **Transfections**

630 For electroporations, 10^7 ESCs were electroporated with 100µg DNA using a BioRad GenePulser set to
631 800V/3µF. For nucleofections, $5x10^5$ ESCs were nucleofected with 5µg DNA with the Lonza P3 Primary
632 Cell Nucleofector Unit and kit, using program CG-104, and following manufacturer instructions. For
633 lipofections, 10^5 ESCs were lipofected with 3µg DNA mixed with 3µl Lipofectamine 3000 and 6µl P3000
634 solution, following manufacturer instructions. For ϕC31-mediated RMCE, equal masses of RMCE
635 constructs and CAG-ϕC31 vector were transfected.

636 Clonal ESC lines were generated by transfecting constructs of interest into ESCs, then plating cells at
637 low density onto gelatinised 9cm dishes in the absence of selection. Selective medium was added 48
638 hours post-transfection and replaced every other day. After 7-10 days, clones were manually picked,
639 dissociated, and replated into gelatinised 96-well culture plates. Clones were transferred to
640 gelatinised vessels with larger culture areas when confluent, screened as appropriate, expanded and
641 cryopreserved.

642 **Cell lines**

643 E14Ju09 ESCs are a 129/Ola male wild-type clonal line derived from E14tg2a (Hamilton and Brickman,
644 2014; Hooper et al., 1987).
645 Sender cells were generated by electroporating E14Ju09 ESCs with one of four constructs: *pPyCAG-*
646 *IgGK signal-EGFP-PDGFRB TMD-IRES-Pac* (CmGP cells), *pPyPGK-IgGK signal-EGFP-PDGFRB TMD-IRES-*
647 *Pac* (PmGP cells), *pPyCAG-IgGK signal-HA-EGFP-Myc-PDGFRB TMD-IRES-Pac* (CHmGMP cells),
648 *pPyPGK-IgGK signal-HA-EGFP-Myc-PDGFRB TMD-IRES-Pac* (PHmGMP cells). Simplified versions of the
649 constructs are displayed in Fig. 2. HA and Myc tags were used in CHmGMP and PHmGMP cell lines as
650 additional markers to identify sender cells, but are not essential given that sender cells can be
651 identified by GFP fluorescence. CmGP1GH1 sender cells were generated by lipofecting CmGP1 sender
652 cells with a *pPyCAG-EGFP-IRES-Hph* construct. E14GIP1 "cytoplasmic sender" cells were generated by
653 lipofecting E14Ju09 ESCs with a *pPyCAG-EGFP-IRES-Pac* construct.
654 EM35 landing pad cells were generated by electroporating E14Ju09 ESCs with the *Rosa26* landing pad
655 targeting vector described above. Correct targeting was verified by genomic DNA PCR with the
656 following primers: Forward: GGCGGACTGGCGGGACTA, Reverse:
657 GGGACAGGATAAGTATGACATCATCAAGG. Primer locations and expected band sizes are displayed in
658 Fig. S3A. This PCR strategy was modified from that described by (Mort et al., 2014) to suit the different
659 sequence of our *Rosa26* targeting vector.
660 SNCB+ and SNCB- receiver cells were generated by electroporating EM35 ESCs with the constructs
661 depicted in Figs. S4A, S6A, and a *CAG-φC31 integrase* construct to mediate RMCE.
662 35SRZ landing pad cells were generated by electroporating EM35 landing pad cells with *pPyPGK-CD8a*
663 *signal-Myc-LaG17-Notch1 minimal transmembrane core-tTA-IRES-Ble*.
664 PSNB landing pad cell lines were generated by nucleofecting 35SRZ ESCs with a *pPyCAG-tagBFP-3xNLS-*
665 *IRES-Hph* construct. PSNB-A cells were derived from 35SRZ clone 9 (PSNB-A clone 10 renamed PSNB
666 clone A), PSNB-B cells were derived from 35SRZ clone 86 (PNSB-B clone 3 renamed PSNB clone B).
667 STC receiver cells were generated by nucleofecting PSNB ESCs with *CAG-φC31 integrase* and the
668 following RMCE construct: *attB53-Pac-bGHpA-(TRE-mCherry-SV40pA)-attB53*. Sequence in brackets is
669 on -strand. STC clone A1 was derived from PSNB clone A, STC clones B1 and B2 were derived from
670 PSNB clone B.
671 PSNB-tetO cells were generated by nucleofecting PSNB ESCs with *CAG-φC31 integrase* and the
672 following RMCE construct: *attB53-Pac-bGHpA-(tetO-mCherry-SV40pA)-attB53*. Sequence in brackets
673 is on -strand.
674 PNSB-E cells were generated by nucleofecting PSNB ESCs with *CAG-φC31 integrase* and the following
675 RMCE construct: *attB53-Pac-bGHpA-attB53*.
676 STN receiver cells were generated by nucleofecting PSNB clone A ESCs with *CAG-φC31 integrase* and
677 the following RMCE construct: *attB53-Pac-bGHpA-(TRE-3xFlag-Neurog1-SV40pA)-attB53*. Sequence in
678 brackets is on -strand.

679 Cell lines generated in this study were routinely karyotyped by chromosome count, checked for
680 absence of mycoplasma infection, and are available on request.

681 **Co-culture experiments**

682 Sender and receiver cells were detached from culture vessels with accutase, quenched in ESC culture
683 medium, pelleted by spinning at 300g for 3 minutes, resuspended in ESC culture medium
684 supplemented with 2µg/ml puromycin and counted. Cells were plated at ratios described in figure
685 legends, and at empirically determined optimal densities.
686 For flow cytometry experiments, cells were plated onto 12-well plates coated with 7.5µg/ml
687 fibronectin, at the following densities: experiments carried out in the absence of doxycyline: 1h-8h:
688 $4x10^5$ cells/well; 16h: $2.4x10^5$ cells/well; 24h: $1.6x10^5$ cells/well; 48h: $8x10^4$ cells/well; 72h: $4x10^4$
689 cells/well. mCherry induction with 16h doxycycline (Fig. 4F-H): 0-4h: $2.4x10^5$ cells/well; 5-8h: $1.6x10^5$
690 cells/well; 24h: $8x10^4$ cells/well. mCherry downregulation experiments (Fig. S14): 0h-8h: $1.6x10^5$
691 cells/well; 16h: $1.2x10^5$ cells/well; 24h: $8x10^4$ cells/well; 48h: $4x10^4$ cells/well.
692 For immunofluorescence experiments, cells were plated on flamed 24mm glass coverslips housed in
693 a 6-well plate coated with 7.5µg/ml fibronectin.
694 For live imaging experiments using a Nikon Ti-E microscope (Movies 1,3-5), cells were plated onto an
695 8-well imaging slide coated with 7.5µg/ml fibronectin, at the following densities: mCherry induction
696 experiments: $3x10^4$ cells/well; mCherry downregulation experiments: 0-24h: $2x10^4$ cells/well; 24-48h:
697 10^4 cells/well. For live imaging experiments using a PerkinElmer Opera Phenix Plus microscope (Movie
698 2, Fig. S16G), cells were plated onto a 96-well imaging plate coated with 7.5µg/ml fibronectin, at the
699 following densities: mCherry induction experiments: $9.6x10^4$ cells/well; mCherry downregulation
700 experiments: 0-24h: $2x10^4$ cells/well; 24-48h: 10^4 cells/well. ESC culture medium was supplemented
701 with 2µg/ml puromycin, 200µg/ml hygromycin B and 1X penicillin/streptomycin.
702 To test induction of 3xFlag-Neurog1 in STN receiver cells, CmGP1 sender cells and STN receiver cells
703 were plated at a 9:1 ratio at a concentration of $2x10^5$ cells/well onto a 24mm flamed glass coverslip
704 housed in a 6-well plate coated with 7.5µg/ml fibronectin, then fixed and stained after 48 hours.

705 **Synthetic patterning experiments**

706 A 24mm glass coverslip housed in a 6-well plate was coated with 7.5µg/ml fibronectin, then allowed
707 to air dry. When fully dry, forceps were used to place a culture insert 3-well silicon chamber on top of
708 the coverslip; downward force was carefully exerted to secure it in place. $4x10^4$ cells were plated
709 overnight in 70µl culture medium in each of the three wells. Sender cells were plated in the central
710 well, and receiver cells were plated in the outside wells. 2ml culture medium were added outside of
711 the 3-well insert in order to prevent evaporation. The next day, the 2ml culture medium outside of
712 the 3-well insert were aspirated, and the 70µl in each of the three wells were carefully removed in
713 order not to dislodge the 3-well insert. Each well was quickly washed with 70µl PBS to get rid of any
714 remaining cells in suspension. Forceps were used to detach the 3-well insert from the glass coverslip,
715 and 2.5ml culture medium were added to the well. Culture medium was replaced daily. Growth of
716 cells into the gaps between wells were monitored daily; following contact between sender and
717 receiver cells, cells were kept in culture for a further 24 hours (STC receivers + CmGP1 senders) or a
718 further 96 hours (STN receivers + CmGP1 senders) prior to fixation and immunofluorescence. For live
719 imaging of mCherry stripe experiments, the 3-well insert was placed in an Ibidi µ-Slide 4 Well instead
720 of on a glass coverslip.

721 **Flow cytometry**

722 Cells were washed in PBS, then detached from culture vessels with accutase. They were resuspended
723 in ice-cold PBS+10% FCS, pelleted by spinning at 300g for 3 minutes, resuspended in ice-cold PBS+10%
724 FCS+300nM DRAQ7 and placed on ice before analysing on a BD LSRFortessa flow cytometer. Forward
725 and side-scatter width and amplitude were used to identify single cells in suspension, dead cells were
726 excluded by gating on DRAQ7-negative cells, and tagBFP, GFP and mCherry/mKate2 expression were
727 then analysed using V 450/50-A, B 530/30-A, Y/G 610/20-A laser/filters combinations respectively.

728 **Immunofluorescence**

729 Cells were plated on flamed glass coverslips coated with 7.5µg/ml fibronectin and cultured as
730 indicated in figure legends. Cells were washed with PBS, fixed in 4% formaldehyde in PBS for 20
731 minutes at room temperature, then washed three times in PBS for a total of 15 minutes. Cells were
732 blocked overnight at 4°C in blocking solution (PBS+3% donkey serum+0.1% Triton X-100). Primary
733 antibodies diluted in blocking solution were added for 3 hours at room temperature, the coverslips
734 were washed 3 times in PBS for a total of 30 minutes, secondary antibodies diluted in blocking solution
735 were added for 1 hour at room temperature, the coverslips were washed 3 times in PBS for a total of
736 30 minutes. The coverslips were then mounted onto glass slides in Prolong Gold mounting medium.
737 For synthetic patterning experiments and chimaera stainings, antibodies were incubated overnight at
738 4°C or 37°C respectively to improve penetration. Blastocysts were imaged in PBS in an imaging
739 chamber, and scoring of mCherry-HI cells was performed manually using chimaeras containing both
740 sender and receiver cells as a reference. Post-implantation chimaeras were were dehydrated in
741 methanol series in PBS/0.1% Triton X-100, clarified in 50% methanol/50% BABB (benzyl alcohol:benzyl
742 benzoate 1:2 ratio), and transferred into 100% BABB before imaging. All imaging was performed on a
743 Leica SP8 confocal microscope with a 40X immersion lens unless otherwise indicated.

744 **Live imaging**

745 Cells to be imaged were allowed to adhere on culture vessels at room temperature for 15 minutes
746 after plating, after which they were placed in a 37°C 5% CO_2 humidified chamber and imaged. For
747 Movies 1, 3-5, imaging was performed with a widefield Nikon Ti-E microscope, 20X lens, and
748 Hamamatsu camera; images were taken at 10-minute intervals for 24 hours, and xy coordinates were
749 saved. Following live imaging, cells were fixed and stained for fluorophore expression, and imaged at
750 the previously saved xy coordinates (Movies 1,3). For Movie 2, Fig. S16G and Fig. S19, imaging was
751 performed with a PerkinElmer Opera PhenixPlus microscope, 20X lens. Images were taken at 1-hour
752 (Movie 2, Fig. S16G) or 90-minute (Fig. S19) intervals for 24 hours. Fully automated segmentation of
753 tagBFP-positive nuclei, tracking, and quantification of fluorescent signal intensity in live imaging
754 experiments was performed using the PerkinElmer Harmony software.

755 Filming of the morula to blastocyst transition was performed with a PerkinElmer Opera PhenixPlus
756 confocal microscope. Sender and receiver cells were placed on opposite poles of morulae, and allowed
757 to aggregate unperturbed for approximately 4 hours prior to imaging, in order to ensure strong
758 binding of ES cells to morulae. They were then transferred to wells of an uncoated Ibidi µ-Slide
759 Angiogenesis imaging slide and imaged. Aside from an initial frame, it was not possible to capture
760 tagBFP signal within the time-lapse movies as embryos were vulnerable to repeated stimulation with
761 ultraviolet light.

762

763 **ACKNOWLEDGEMENTS**

764 We thank Leonardo Morsut and Wendell Lim for developing the original SynNotch system, Elise Cachat
765 and Keisuke Kaji for advice and reagents, Luis Ángel Fernández for the pDisplay-EGFP-TM plasmid,
766 Andras Nagy for the CAG-ϕC31 plasmid, Dónal O'Carroll and Pedro Moreira for assistance with
767 generating chimaeric mice, Eve Moutaux for cloning initial versions of the RMCE constructs, Alexandre
768 Veiga and Matthew French for performing preliminary experiments with the original SynNotch
769 constructs. We thank Justyna Cholewa-Waclaw, Matthieu Vermeren and Charles Williams for
770 assistance with time-lapse imaging, Fiona Rossi and Claire Cryer for flow cytometry support, and

Theresa O'Connor, Helen Henderson and Marilyn Thomson for cell culture support. We are grateful to Leonardo Morsut and members of the Lowell and Wilson labs for helpful discussions.

COMPETING INTERESTS

The authors declare no competing interests.

FUNDING

This work was funded by a Wellcome Trust Senior Fellowship to SL (WT103789AIA) and a Wellcome Trust Sir Henry Wellcome Fellowship to GB (WT100133).

REFERENCES

Armingol, E., Officer, A., Harismendy, O. and Lewis, N. E. (2021). Deciphering cell–cell interactions and communication from gene expression. *Nature Reviews Genetics* **22**, 71–88.

Arnold, S. J. and Robertson, E. J. (2009). Making a commitment: cell lineage allocation and axis patterning in the early mouse embryo. *Nature Reviews Molecular Cell Biology* **10**, 91–103.

Blin, G., Wisniewski, D., Picart, C., Thery, M., Puceat, M. and Lowell, S. (2018). Geometrical confinement controls the asymmetric patterning of Brachyury in cultures of pluripotent cells. *Development*.

Blin, G., Sadurska, D., Migueles, R. P., Chen, N., Watson, J. A. and Lowell, S. (2019). Nessys: A new set of tools for the automated detection of nuclei within intact tissues and dense 3D cultures. *PLOS Biol.* **17**, e3000388.

Boggs, S. S., Gregg, R. G., Borenstein, N. and Smithies, O. (1986). Efficient transformation and frequent single-site, single-copy insertion of DNA can be obtained in mouse erythroleukemia cells transformed by electroporation. *Experimental Hematology* **14**, 988–994.

Bradley, A., Evans, M., Kaufman, M. H. and Robertson, E. (1984). Formation of germ-line chimaeras from embryo-derived teratocarcinoma cell lines. *Nature* **309**, 255–256.

Cachat, E., Liu, W., Martin, K. C., Yuan, X., Yin, H., Hohenstein, P. and Davies, J. A. (2016). 2- and 3-dimensional synthetic large-scale de novo patterning by mammalian cells through phase separation. *Sci. Rep.* **6**, 20664.

Cai, L., Morrow, E. M. and Cepko, C. L. (2000). Misexpression of basic helix-loop-helix genes in the murine cerebral cortex affects cell fate choices and neuronal survival. *Development* **127**, 3021–3030.

Cau, E., Casarosa, S. and Guillemot, F. (2002). Mash1 and Ngn1 control distinct steps of determination and differentiation in the olfactory sensory neuron lineage. *Development* **129**, 1871–1880.

807 **Charrier, S., Ferrand, M., Zerbato, M., Précigout, G., Viornery, A., Bucher-Laurent, S., Benkhelifa-**
808 **Ziyyat, S., Merten, O. W., Perea, J. and Galy, A.** (2011). Quantification of lentiviral vector
809 copy numbers in individual hematopoietic colony-forming cells shows vector dose-
810 dependent effects on the frequency and level of transduction. *Gene Therapy* **18**, 479–487.

811 **Chen, C., Krohn, J., Bhattacharya, S. and Davies, B.** (2011). A Comparison of Exogenous Promoter
812 Activity at the ROSA26 Locus Using a PhiC31 Integrase Mediated Cassette Exchange
813 Approach in Mouse ES Cells. *PLOS ONE* **6**, e23376.

814 **Cho, J. H., Okuma, A., Al-Rubaye, D., Intisar, E., Junghans, R. P. and Wong, W. W.** (2018).
815 Engineering Axl specific CAR and SynNotch receptor for cancer therapy. *Scientific Reports* **8**,
816 3846.

817 **Choe, J. H., Watchmaker, P. B., Simic, M. S., Gilbert, R. D., Li, A. W., Krasnow, N. A., Downey, K. M.,**
818 **Yu, W., Carrera, D. A., Celli, A., et al.** (2021). SynNotch-CAR T cells overcome challenges of
819 specificity, heterogeneity, and persistence in treating glioblastoma. *Sci Transl Med* **13**,.

820 **Davies, J.** (2017). Using synthetic biology to explore principles of development. *Development* **144**,
821 1146–1158.

822 **De Los Angeles, A., Ferrari, F., Xi, R., Fujiwara, Y., Benvenisty, N., Deng, H., Hochedlinger, K.,**
823 **Jaenisch, R., Lee, S., Leitch, H. G., et al.** (2015). Hallmarks of pluripotency. *Nature* **525**, 469–
824 478.

825 **Dias, A. S., Almeida, I. de, Belmonte, J. M., Glazier, J. A. and Stern, C. D.** (2014). Somites Without a
826 Clock. *Science* **343**, 791–795.

827 **Ebrahimkhani, M. R. and Ebisuya, M.** (2019). Synthetic developmental biology: build and control
828 multicellular systems. *Curr. Opin. Chem. Biol.* **52**, 9–15.

829 **Evans, M. J. and Kaufman, M. H.** (1981). Establishment in culture of pluripotential cells from mouse
830 embryos. *Nature* **292**, 154–156.

831 **Fischer, S. C., Corujo-Simon, E., Lilao-Garzon, J., Stelzer, E. H. K. and Muñoz-Descalzo, S.** (2020). The
832 transition from local to global patterns governs the differentiation of mouse blastocysts.
833 *PLOS ONE* **15**, e0233030.

834 **Forsyth, J. E., Al-Anbaki, A. H., Fuente, R. de la, Modare, N., Perez-Cortes, D., Rivera, I., Kelly, R. S.,**
835 **Cotter, S. and Plusa, B.** (2021). IVEN: A quantitative tool to describe 3D cell position and
836 neighbourhood reveals architectural changes in FGF4-treated preimplantation embryos.
837 *PLOS Biology* **19**, e3001345.

838 **Fridy, P. C., Li, Y., Keegan, S., Thompson, M. K., Nudelman, I., Scheid, J. F., Oeffinger, M.,**
839 **Nussenzweig, M. C., Fenyö, D., Chait, B. T., et al.** (2014). A robust pipeline for rapid
840 production of versatile nanobody repertoires. *Nature Methods* **11**, 1253–1260.

841 **Friedrich, G. and Soriano, P.** (1991). Promoter traps in embryonic stem cells: a genetic screen to
842 identify and mutate developmental genes in mice. *Gene Dev* **5**, 1513–1523.

843 **Gorfinkiel, N. and Martinez Arias, A.** (2021). The cell in the age of the genomic revolution: Cell
844 Regulatory Networks. *Cells & Development* 203720.

845 **Gossen, M. and Bujard, H.** (1992). Tight control of gene expression in mammalian cells by
846 tetracycline-responsive promoters. *Proceedings of the National Academy of Sciences* **89**,
847 5547–5551.

848 **Gurdon, J. B.** (1987). Embryonic induction — molecular prospects. *Development* **99**, 285–306.

849 **Hamilton, W. B. and Brickman, J. M.** (2014). Erk signaling suppresses embryonic stem cell self-
850 renewal to specify endoderm. *Cell Reports* **9**, 2056–2070.

851 **Han, H.-J., Park, S.-G., Kim, S.-H., Hwang, S.-Y., Han, J., Traicoff, J., Kho, W.-G. and Chung, J.-Y.**
852 (2004). Epidermal growth factor-like motifs 1 and 2 of Plasmodium vivax merozoite surface
853 protein 1 are critical domains in erythrocyte invasion. *Biochemical and Biophysical Research*
854 *Communications* **320**, 563–570.

855 **He, L., Huang, J. and Perrimon, N.** (2017). Development of an optimized synthetic Notch receptor as
856 an in vivo cell–cell contact sensor. *Proc. Natl. Acad. Sci.* **114**, 5467–5472.

857 **Herbst, F., Ball, C. R., Tuorto, F., Nowrouzi, A., Wang, W., Zavidij, O., Dieter, S. M., Fessler, S.,**
858 **Hoeven, F. van der, Kloz, U., et al.** (2012). Extensive Methylation of Promoter Sequences
859 Silences Lentiviral Transgene Expression During Stem Cell Differentiation In Vivo. *Molecular*
860 *Therapy* **20**, 1014–1021.

861 **Ho, C. and Morsut, L.** (2021). Novel synthetic biology approaches for developmental systems. *Stem*
862 *Cell Reports* **16**, 1051–1064.

863 **Hong, S., Hwang, D.-Y., Yoon, S., Isacson, O., Ramezani, A., Hawley, R. G. and Kim, K.-S.** (2007).
864 Functional Analysis of Various Promoters in Lentiviral Vectors at Different Stages of In Vitro
865 Differentiation of Mouse Embryonic Stem Cells. *Molecular Therapy* **15**, 1630–1639.

866 **Hooper, M., Hardy, K., Handyside, A., Hunter, S. and Monk, M.** (1987). HPRT-deficient (Lesch–
867 Nyhan) mouse embryos derived from germline colonization by cultured cells. *Nature* **326**,
868 292–295.

869 **Huang, J., Zhou, W., Dong, W., Watson, A. M. and Hong, Y.** (2009). Directed, efficient, and versatile
870 modifications of the Drosophila genome by genomic engineering. *Proceedings of the*
871 *National Academy of Sciences* **106**, 8284–8289.

872 **Huang, H., Zhang, X., Lv, J., Yang, H., Wang, X., Ma, S., Shao, R., Peng, X., Lin, Y. and Rong, Z.**
873 (2020). Cell-cell contact-induced gene editing/activation in mammalian cells using a
874 synNotch-CRISPR/Cas9 system. *Protein & Cell* **11**, 299–303.

875 **Johnson, M. H. and Ziomek, C. A.** (1983). Cell interactions influence the fate of mouse blastomeres
876 undergoing the transition from the 16- to the 32-cell stage. *Developmental Biology* **95**, 211–
877 218.

878 **Kinoshita, M. and Smith, A.** (2018). Pluripotency Deconstructed. *Development, Growth &*
879 *Differentiation* **60**, 44–52.

880 **Kinoshita, N., Huang, A. J. Y., McHugh, T. J., Miyawaki, A. and Shimogori, T.** (2020). Diffusible
881 GRAPHIC to visualize morphology of cells after specific cell–cell contact. *Scientific Reports* **10**,
882 14437.

883 **Kondoh, G., Gao, X.-H., Nakano, Y., Koike, H., Yamada, S., Okabe, M. and Takeda, J.** (1999). Tissue-
884 inherent fate of GPI revealed by GPI-anchored GFP transgenesis. *FEBS Letters* **458**, 299–303.

885 **Liew, C.-G., Draper, J. S., Walsh, J., Moore, H. and Andrews, P. W.** (2007). Transient and Stable
886 Transgene Expression in Human Embryonic Stem Cells. *Stem Cells* **25**, 1521–1528.

887 **Luo, H., Wu, X., Sun, R., Su, J., Wang, Y., Dong, Y., Shi, B., Sun, Y., Jiang, H. and Li, Z.** (2019). Target-
888 Dependent Expression of IL12 by synNotch Receptor-Engineered NK92 Cells Increases the
889 Antitumor Activities of CAR-T Cells. *Frontiers in Oncology* **9**,.

890 **Ma, Q., Kintner, C. and Anderson, D. J.** (1996). Identification of neurogenin, a Vertebrate Neuronal
891 Determination Gene. *Cell* **87**, 43–52.

892 **Ma, Q., Chen, Z., Barrantes, I. del B., Pompa, J. L. de la and Anderson, D. J.** (1998). neurogenin1 Is
893 Essential for the Determination of Neuronal Precursors for Proximal Cranial Sensory Ganglia.
894 *Neuron* **20**, 469–482.

895 **Malaguti, M., Nistor, P. A., Blin, G., Pegg, A., Zhou, X. and Lowell, S.** (2013). Bone morphogenic
896 protein signalling suppresses differentiation of pluripotent cells by maintaining expression of
897 E-Cadherin. *eLife* **2**, e01197.

898 **Malaguti, M., Migueles, R. P., Blin, G., Lin, C.-Y. and Lowell, S.** (2019). Id1 Stabilizes Epiblast Identity
899 by Sensing Delays in Nodal Activation and Adjusting the Timing of Differentiation. *Dev. Cell*
900 **50**, 462–477.e5.

901 **Martin, G. R.** (1981). Isolation of a pluripotent cell line from early mouse embryos cultured in
902 medium conditioned by teratocarcinoma stem cells. *Proceedings of the National Academy of*
903 *Sciences* **78**, 7634–7638.

904 **Matsuda, M., Koga, M., Woltjen, K., Nishida, E. and Ebisuya, M.** (2015). Synthetic lateral inhibition
905 governs cell-type bifurcation with robust ratios. *Nat Commun* **6**, 6195.

906 **Matsunaga, S., Jeremiah, S. S., Miyakawa, K., Kurotaki, D., Shizukuishi, S., Watashi, K., Nishitsuji,**
907 **H., Kimura, H., Tamura, T., Yamamoto, N., et al.** (2020). Engineering Cellular Biosensors
908 with Customizable Antiviral Responses Targeting Hepatitis B Virus. *iScience* **23**,.

909 **McBurney, M. W., Sutherland, L. C., Adra, C. N., Leclair, B., Rudnicki, M. A. and Jardine, K.** (1991).
910 The mouse Pgk-1 gene promoter contains an upstream activator sequence. *Nucleic Acids*
911 *Research* **19**, 5755–5761.

912 **Monetti, C., Nishino, K., Biechele, S., Zhang, P., Baba, T., Woltjen, K. and Nagy, A.** (2011). PhiC31
913 integrase facilitates genetic approaches combining multiple recombinases. *Methods* **53**,
914 380–385.

915 **Morsut, L., Roybal, K. T., Xiong, X., Gordley, R. M., Coyle, S. M., Thomson, M. and Lim, W. A.**
916 (2016). Engineering Customized Cell Sensing and Response Behaviors Using Synthetic Notch
917 Receptors. *Cell* **164**, 780–791.

918 **Mort, R. L., Ford, M. J., Sakaue-Sawano, A., Lindstrom, N. O., Casadio, A., Douglas, A. T., Keighren,**
919 **M. A., Hohenstein, P., Miyawaki, A. and Jackson, I. J.** (2014). Fucci2a: A bicistronic cell cycle
920 reporter that allows Cre mediated tissue specific expression in mice. *Cell Cycle* **13**, 2681–
921 2696.

922 **Nishida-Aoki, N. and Gujral, T. S.** (2019). Emerging approaches to study cell-cell interactions in
923 tumor microenvironment. *Oncotarget* **10**, 785–797.

924 **Niwa, H., Yamamura, K. and Miyazaki, J.** (1991). Efficient selection for high-expression transfectants
925 with a novel eukaryotic vector. *Gene* **108**, 193–199.

926 **Nowotschin, S. and Hadjantonakis, A.-K.** (2010). Cellular dynamics in the early mouse embryo: from
927 axis formation to gastrulation. *Current Opinion in Genetics & Development* **20**, 420–427.

928 **Nowotschin, S., Eakin, G. S. and Hadjantonakis, A.-K.** (2009). Dual transgene strategy for live
929 visualization of chromatin and plasma membrane dynamics in murine embryonic stem cells
930 and embryonic tissues. *genesis* **47**, 330–336.

931 **Ombrato, L., Nolan, E., Kurelac, I., Mavousian, A., Bridgeman, V. L., Heinze, I., Chakravarty, P.,**
932 **Horswell, S., Gonzalez-Gualda, E., Matacchione, G., et al.** (2019). Metastatic-niche labelling
933 reveals parenchymal cells with stem features. *Nature* **572**, 603–608.

934 **Pera, M. F. and Tam, P. P. L.** (2010). Extrinsic regulation of pluripotent stem cells. *Nature* **465**, 713–
935 720.

936 **Perez, S. E., Rebelo, S. and Anderson, D. J.** (1999). Early specification of sensory neuron fate
937 revealed by expression and function of neurogenins in the chick embryo. *Development* **126**,
938 1715–1728.

939 **Pfaff, N., Lachmann, N., Ackermann, M., Kohlscheen, S., Brendel, C., Maetzig, T., Niemann, H.,**
940 **Antoniou, M. N., Grez, M., Schambach, A., et al.** (2013). A ubiquitous chromatin opening
941 element prevents transgene silencing in pluripotent stem cells and their differentiated
942 progeny. *STEM CELLS* **31**, 488–499.

943 **Pfeifer, A., Ikawa, M., Dayn, Y. and Verma, I. M.** (2002). Transgenesis by lentiviral vectors: lack of
944 gene silencing in mammalian embryonic stem cells and preimplantation embryos.
945 *Proceedings of the National Academy of Sciences of the United States of America* **99**, 2140–
946 2145.

947 **Posfai, E., Lanner, F., Mulas, C. and Leitch, H. G.** (2021). All models are wrong, but some are useful:
948 Establishing standards for stem cell-based embryo models. *Stem Cell Reports* **16**, 1117–1141.

949 **Rao, C., Malaguti, M., Mason, J. O. and Lowell, S.** (2020). The transcription factor E2A drives neural
950 differentiation in pluripotent cells. *Development*.

951 **Rhee, J. M., Pirity, M. K., Lackan, C. S., Long, J. Z., Kondoh, G., Takeda, J. and Hadjantonakis, A.-K.**
952 (2006). In vivo imaging and differential localization of lipid-modified GFP-variant fusions in
953 embryonic stem cells and mice. *genesis* **44**, 202–218.

954 **Rossant, J. and Tam, P. P. L.** (2009). Blastocyst lineage formation, early embryonic asymmetries and
955 axis patterning in the mouse. *Development* **136**, 701–713.

956 **Roybal, K. T., Williams, J. Z., Morsut, L., Rupp, L. J., Kolinko, I., Choe, J. H., Walker, W. J., McNally,**
957 **K. A. and Lim, W. A.** (2016). Engineering T Cells with Customized Therapeutic Response
958 Programs Using Synthetic Notch Receptors. *Cell* **167**, 419–432.e16.

959 **Sancho, M., Di-Gregorio, A., George, N., Pozzi, S., Sánchez, J. M., Pernaute, B. and Rodríguez, T. A.**
960 (2013). Competitive Interactions Eliminate Unfit Embryonic Stem Cells at the Onset of
961 Differentiation. *Developmental Cell* **26**, 19–30.

962 **Santorelli, M., Lam, C. and Morsut, L.** (2019). Synthetic development: building mammalian
963 multicellular structures with artificial genetic programs. *Curr Opin Biotechnol* **59**, 130–140.

964 **Schlissel, G. and Li, P.** (2020). Synthetic Developmental Biology: Understanding Through
965 Reconstitution. *Annu. Rev. Cell Dev. Biol.* **36**, 339–357.

966 **Schultz, R. M.** (1985). Roles of Cell-to-Cell Communication in Development. *Biology of Reproduction*
967 **32**, 27–42.

968 **Seibler, J., Küter-Luks, B., Kern, H., Streu, S., Plum, L., Mauer, J., Kühn, R., Brüning, J. C. and**
969 **Schwenk, F.** (2005). Single copy shRNA configuration for ubiquitous gene knockdown in
970 mice. *Nucleic Acids Research* **33**, e67–e67.

971 **Sekine, R., Shibata, T. and Ebisuya, M.** (2018). Synthetic mammalian pattern formation driven by
972 differential diffusivity of Nodal and Lefty. *Nat Commun* **9**, 5456.

973 **Sevcsik, E., Brameshuber, M., Fölser, M., Weghuber, J., Honigmann, A. and Schütz, G. J.** (2015).
974 GPI-anchored proteins do not reside in ordered domains in the live cell plasma membrane.
975 *Nature Communications* **6**, 6969.

976 **Sgodda, M., Alfken, S., Schambach, A., Eggenschwiler, R., Fidzinski, P., Hummel, M. and Cantz, T.**
977 (2020). Synthetic Notch-Receptor-Mediated Transmission of a Transient Signal into
978 Permanent Information via CRISPR/Cas9-Based Genome Editing. *Cells* **9**, 1929.

979 **Shcherbo, D., Murphy, C. S., Ermakova, G. V., Solovieva, E. A., Chepurnykh, T. V., Shcheglov, A. S.,**
980 **Verkhusha, V. V., Pletnev, V. Z., Hazelwood, K. L., Roche, P. M., et al.** (2009). Far-red
981 fluorescent tags for protein imaging in living tissues. *Biochemical Journal* **418**, 567–574.

982 **Shioi, G., Kiyonari, H., Abe, T., Nakao, K., Fujimori, T., Jang, C.-W., Huang, C.-C., Akiyama, H.,**
983 **Behringer, R. R. and Aizawa, S.** (2011). A mouse reporter line to conditionally mark nuclei
984 and cell membranes for in vivo live-imaging. *Genesis* **49**, 570–578.

985 **Smithies, O., Gregg, R. G., Boggs, S. S., Koralewski, M. A. and Kucherlapati, R. S.** (1985). Insertion of
986 DNA sequences into the human chromosomal ß-globin locus by homologous recombination.
987 *Nature* **317**, 230–234.

988 **Srivastava, S., Salter, A. I., Liggitt, D., Yechan-Gunja, S., Sarvothama, M., Cooper, K., Smythe, K. S.,**
989 **Dudakov, J. A., Pierce, R. H., Rader, C., et al.** (2019). Logic-Gated ROR1 Chimeric Antigen
990 Receptor Expression Rescues T Cell-Mediated Toxicity to Normal Tissues and Enables
991 Selective Tumor Targeting. *Cancer Cell* **35**, 489–503.e8.

992 **Stern, C.** (1936). Somatic Crossing Over and Segregation in Drosophila Melanogaster. *Genetics* **21**,
993 625–730.

994 **Tam, P. P. L. and Loebel, D. A. F.** (2007). Gene function in mouse embryogenesis: get set for
995 gastrulation. *Nature Reviews Genetics* **8**, 368–381.

Tang, R., Murray, C. W., Linde, I. L., Kramer, N. J., Lyu, Z., Tsai, M. K., Chen, L. C., Cai, H., Gitler, A. D., Engleman, E., et al. (2020). A versatile system to record cell-cell interactions. *eLife* **9**, e61080.

Tchorz, J. S., Suply, T., Ksiazek, I., Giachino, C., Cloëtta, D., Danzer, C.-P., Doll, T., Isken, A., Lemaistre, M., Taylor, V., et al. (2012). A Modified RMCE-Compatible Rosa26 Locus for the Expression of Transgenes from Exogenous Promoters. *PLOS ONE* **7**, e30011.

Toda, S., Blauch, L. R., Tang, S. K. Y., Morsut, L. and Lim, W. A. (2018). Programming self-organizing multicellular structures with synthetic cell-cell signaling. *Science* **361**, 156–162.

Toda, S., McKeithan, W. L., Hakkinen, T. J., Lopez, P., Klein, O. D. and Lim, W. A. (2020). Engineering synthetic morphogen systems that can program multicellular patterning. *Science* **370**, 327–331.

Tosti, L., Ashmore, J., Tan, B. S. N., Carbone, B., Mistri, T. K., Wilson, V., Tomlinson, S. R. and Kaji, K. (2018). Mapping transcription factor occupancy using minimal numbers of cells in vitro and in vivo. *Genome Research* **28**, 592–605.

Toth, T., Balassa, T., Bara, N., Kovacs, F., Kriston, A., Molnar, C., Haracska, L., Sukosd, F. and Horvath, P. (2018). Environmental properties of cells improve machine learning-based phenotype recognition accuracy. *Scientific Reports* **8**, 10085.

Velkey, J. M. and O'Shea, K. S. (2013). Expression of Neurogenin 1 in Mouse Embryonic Stem Cells Directs the Differentiation of Neuronal Precursors and Identifies Unique Patterns of Downstream Gene Expression. *Developmental Dynamics* **242**, 230–253.

Wang, L., Long, J., Chen, H., Sun, S., Lv, K., Li, Q. and Wang, X. (2021). Manipulation of focal Wnt activity via synthetic cells in a double-humanized zebrafish model of tumorigenesis. *International Journal of Cancer* **148**, 2815–2824.

Whittingham, D. G. (1974). Embryo banks in the future of developmental genetics. *Genetics* **78**, 395–402.

Wu, G., Liu, N., Rittelmeyer, I., Sharma, A. D., Sgodda, M., Zaehres, H., Bleidißel, M., Greber, B., Gentile, L., Han, D. W., et al. (2011). Generation of Healthy Mice from Gene-Corrected Disease-Specific Induced Pluripotent Stem Cells. *PLOS Biology* **9**, e1001099.

Yang, Z., Yu, Z., Cai, Y., Du, R. and Cai, L. (2020). Engineering of an enhanced synthetic Notch receptor by reducing ligand-independent activation. *Communications Biology* **3**, 1–7.

Yang, B. A., Westerhof, T. M., Sabin, K., Merajver, S. D. and Aguilar, C. A. (2021). Engineered Tools to Study Intercellular Communication. *Advanced Science* **8**, 2002825.

Yuan, L. and Hassan, B. A. (2014). Neurogenins in brain development and disease: An overview. *Archives of Biochemistry and Biophysics* **558**, 10–13.

Zhu, I., Liu, R., Hyrenius-Wittsten, A., Piraner, D. I., Alavi, J., Israni, D. V., Khalil, A. S. and Roybal, K. T. (2021). Design and modular assembly of synthetic intramembrane proteolysis receptors for custom gene regulation in therapeutic cells. *bioRxiv* 2021.05.21.445218.

1034 **FIGURE LEGENDS**

1035 **Figure 1. Diagram of SynNotch cell-cell interaction reporter ES cells.**
1036 (A) Interaction between a membrane-tethered ligand and the Notch receptor extracellular domain
1037 leads to the cleavage of the Notch core transmembrane domain, which contains proteolytic cleavage
1038 sites. In turn, this leads to the release of the Notch intracellular domain from the membrane,
1039 allowing it to translocate to the nucleus and drive transcription of target genes. (B) Sender cells
1040 express membrane-tethered extracellular EGFP from a ubiquitous promoter. (C) Receiver cells
1041 contain a *TRE-mCherry* transgene, express *tagBFP-3xNLS* from a ubiquitous promoter, and express a
1042 SynNotch receptor from a ubiquitous promoter. The SynNotch receptor is comprised of an
1043 extracellular LaG17 anti-GFP nanobody, the core transmembrane region of Notch1, and an
1044 intracellular tTA. (D) Upon interaction of the EGFP on a sender cell with the SynNotch receptor, the
1045 Notch1 core domain is cleaved, releasing the tTA, which can translocate into the nucleus, bind the
1046 TRE element, and drive *mCherry* transcription.

1047 **Figure 2. Screening of clonal sender ESC lines.**
1048 (A-D) Diagram of the constructs used to generate EGFP sender cell lines. (E) Median EGFP intensity
1049 and (G) percentage EGFP-positive cells in untagged EGFP sender cells. Parental wild-type cells are
1050 included as a negative control. 5000 cells were analysed for each clone. (F) Median EGFP intensity
1051 and (H) percentage EGFP-positive cells in HA- and Myc-tagged EGFP sender cells. Parental wild-type
1052 cells are included as a negative control. 15000 cells were analysed for each clone. Analyses were
1053 performed separately from those in (E), median intensities are not directly comparable. For panels
1054 (E-H), n=1. (I) Comparison of EGFP distributions in parental wild-type cells, CmGP clone 1 (CmGP1)
1055 and CHmGMP clone 19 (CHmGMP19) sender cells. 85000 cells were analysed for each sample. Data
1056 from a single experiment, representative of 9 biological replicates. (J) Immunofluorescence of
1057 parental wild-type, CmGP1 and CHmGMP19 sender cells. Scale bar: 30µm. Nuclei: LaminB1. A.F.U.:
1058 arbitrary fluorescence units.

1059 **Figure 3. Generation of clonal cell-cell interaction reporter STC receiver cells.**
1060 (A) Summary of transgenes stably integrated into the genome of STC clonal ESC lines. (B-C) Flow
1061 cytometry analysis of mCherry and tagBFP-3xNLS expression in (B) wild-type and (C) control PSNBB-E
1062 cells containing all SyNPL receiver constructs except for the TRE-mCherry cassette. These control cell
1063 lines were used to set gates for tagBFP- and mCherry-positivity. (D) Immunofluorescence of STC
1064 clones A1, B1 and B2 co-cultured with CmGP1 sender cells for 24 hours (1:3 sender:receiver cell
1065 ratio). Scale bar: 30µm. (E-H) Flow cytometry analysis of mCherry and tagBFP-3xNLS expression in
1066 STC receiver cells cultured alone or in the presence of indicated EGFP-expressing cell lines (9:1
1067 sender:receiver cell ratio). The mCherry-HI gate displayed in figure was set based on mCherry
1068 distribution in STC receiver cells cultured alone. Data in these panels were acquired simultaneously
1069 to data in panels (B,C) and can be directly compared.
1070 For panels (B,C,E-H) percentages of cells in each gate are indicated. 11000 cells were analysed for
1071 each sample. Data from a single experiment, representative of 4 biological replicates. Diagrams
1072 depicting the transgenes present in each cell type and expected mCherry and tagBFP-3xNLS
1073 expression patterns are displayed next to flow cytometry plots.

1074 **Figure 4. Kinetics of mCherry induction in STC receiver cells.**
1075 (A) Stills from Movie 1 displaying mCherry and EGFP expression in STC clone A1 receiver cells co-
1076 cultured with CmGP1GH1 sender cells (1:1 sender:receiver cell ratio). Immuofluorescence of cells
1077 after 24 hours of filming is displayed as a 24 hour timepoint, and includes tagBFP-3xNLS signal in
1078 place of a brightfield image. Scale bar: 30µm. Yellow arrowheads: initial STC receiver cell contact
1079 with sender cells, onset of mCherry expression, cell descendants at 24 hours. Magenta arrowheads:
1080 STC receiver cell not making contact with sender cells, cell descendants at 24 hours. Cyan
1081 arrowhead: initial STC receiver cell contact with sender cell, cell descendant at 24 hours.

1082 (B) Stills from Movie 2 displaying tagBFP-3xNLS, mCherry and EGFP expression in STC clone A1
1083 receiver cells co-cultured with CmGP1GH1 sender cells (9:1 sender:receiver cell ratio). Scale bar:
1084 30µm.
1085 (C) Experimental setup to analyse kinetics of mCherry upregulation in STC receiver cells by flow
1086 cytometry.
1087 (D) Percentage of mCherry-HI STC receiver cells following co-culture with CmGP1 sender cells for the
1088 indicated amount of time (9:1 sender:receiver cell ratio). Data presented as mean ± standard
1089 deviation of three independent experiments. A minimum of 8000 cells were analysed for each
1090 sample. The mCherry-HI gate was set based on mCherry distribution in STC receiver cells cultured
1091 alone.
1092 (E) Distribution of mCherry fluorescence in STC clone A1 receiver cells following co-culture with
1093 CmGP1 sender cells for the indicated amount of time (9:1 sender:receiver cell ratio). Data from a
1094 single experiment, representative of three biological replicates. STC clone A1 cells cultured alone
1095 ("0h") are displayed as a shaded black histogram in all panels. 10000 cells were analysed for each
1096 sample.
1097 (F) Quantification of live imaging: median mCherry fluorescence intensity in STC clone A1 receiver
1098 cells following co-culture with CmGP1GH1 or E14GIP1 cells for the indicated amount of time (9:1
1099 sender:receiver cell ratio). Average of 3 biological replicates, 10 random fields of view/replicate,
1100 minimum of 320 cells/replicate/timepoint. Error bars: standard deviation.
1101 (G) Mean mCherry fluorescence intensity in individual STC clone A1 receiver cells tracked for 24
1102 hours whilst in co-culture with CmGP1GH1 sender cells (9:1 sender:receiver ratio). Tracks are
1103 displayed for 33 randomly selected cells for each of 3 biological replicates (99 cells total). Mean, 10th,
1104 and 90th centile tracks are also displayed.
1105 A.F.U.: arbitrary fluorescence units.
1106
1107 **Figure 5. Characterisation of minimal contact time required for mCherry induction in STC receiver**
1108 **cells.**
1109 (A) Stills from Movie 3 displaying mCherry and EGFP expression in STC clone A1 receiver cells co-
1110 cultured with CmGP1GH1 sender cells (1:1 sender:receiver cell ratio). Immuofluorescence of cells
1111 after 24 hours of filming is displayed as a 24 hour timepoint, and includes tagBFP-3xNLS signal in
1112 place of a brightfield image. Scale bar: 30µm. White arrowheads label an STC receiver cell in contact
1113 with sender cells for 7 hours, which then loses contact with sender cells between the 8 and 20 hour
1114 timepoints whilst its levels of mCherry keep increasing. (B) Experimental setup to analyse kinetics of
1115 mCherry upregulation in STC receiver cells by flow cytometry, allowing time for protein maturation.
1116 Following sender:receiver cell co-culture for 0-24 hours, 1µg/ml doxycycline (dox) was added to the
1117 culture medium for a further 16 hours in order to inhibit tTA-mediated *mCherry* transcription, and
1118 allow translation and folding of previously transcribed *mCherry*.
1119 (C) Percentage of mCherry-HI STC receiver cells after co-culture with CmGP1 sender cells for the
1120 indicated amount of time and following a further 16 hours of doxycycline treatment (9:1
1121 sender:receiver cell ratio). Data presented as mean ± standard deviation of three independent
1122 experiments. A minimum of 8000 cells were analysed for each sample. The mCherry-HI gate was set
1123 based on mCherry distribution in STC receiver cells cultured alone in doxycycline for 16 hours.
1124 (D) Distribution of mCherry fluorescence in STC clone A1 receiver cells following co-culture with
1125 CmGP1 sender cells for the indicated amount of time and 16 hours doxycycline treatment (9:1
1126 sender:receiver cell ratio). Data from a single experiment, representative of three biological
1127 replicates. STC clone A1 cells plated with CmGP1 sender cells in doxycycline-containing medium for
1128 16 hours ("0h") are displayed as a shaded black histogram in all panels. 10000 cells were analysed
1129 for each sample.
1130
1131 **Figure 6. Contact-mediated induction of mCherry in chimaeric blastocysts.**

1132 (A) Chimaeric blastocysts containing STC clone B1 receiver cells and/or CmGP1GH1 sender cells. The
1133 images of the three embryos were taken from the same z-plane of a confocal stack and come from a
1134 single field of view. Nuclei were counterstained with DRAQ7. Scale bars: 30µm. (B) Quantification of
1135 embryos containing cells expressing readily detectable levels of mCherry ("mCherry-HI") across all
1136 experiments. Embryos containing both sender and receiver cells were used as a reference for scoring
1137 sender-only chimaeras, receiver-only chimaeras, and wild-type embryos.

1138 **Figure 7. Contact-mediated synthetic patterning of gene expression and fate programming.**
1139 (A) Diagram illustrating synthetic patterning strategy: sender and receiver cells are grown to
1140 confluence in separate chambers of a multi-chamber culture insert. The insert is removed and cells
1141 are allowed to proliferate until they come into contact, which induces transgene expression in
1142 receiver cells in a stripe pattern. (B) Synthetic striped pattern of mCherry induction in STC clone B1
1143 receiver ESCs in contact with CmGP1 sender ESCs. EGFP, tagBFP, mCherry immunofluorescence. (C)
1144 Summary of transgenes stably integrated into the genome of *Neurog1*-inducible STN clonal ESC lines.
1145 (D) Synthetic striped pattern of neuronal differentiation of STN receiver ES cells in contact with
1146 CmGP1 sender ESCs. EGFP, tagBFP, Tubb3 immunofluorescence. Scale bars: 30µm.

FIGURE 1

A Notch signalling

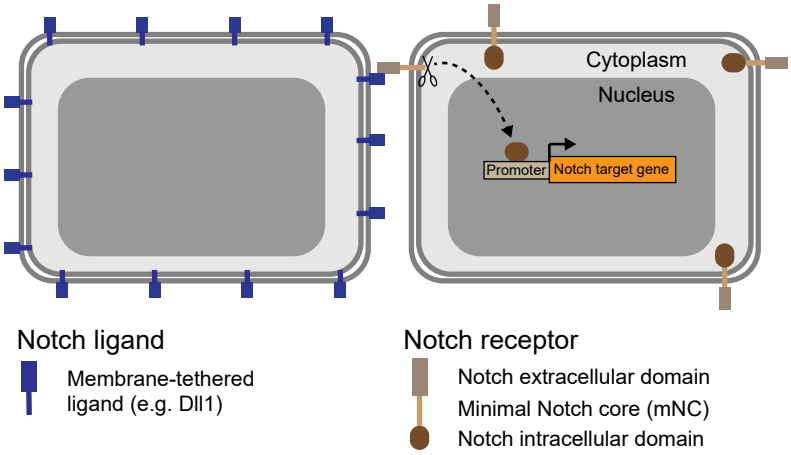

B SyNPL sender cells

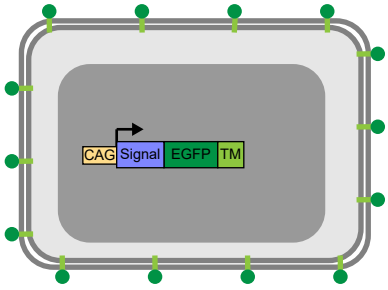

C SyNPL receiver cells

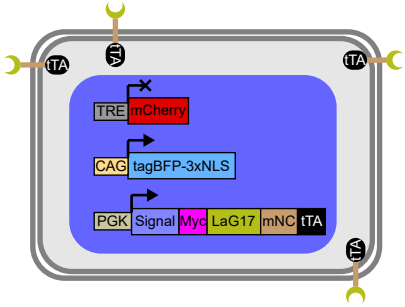

D Sender cells in direct contact with receiver cells

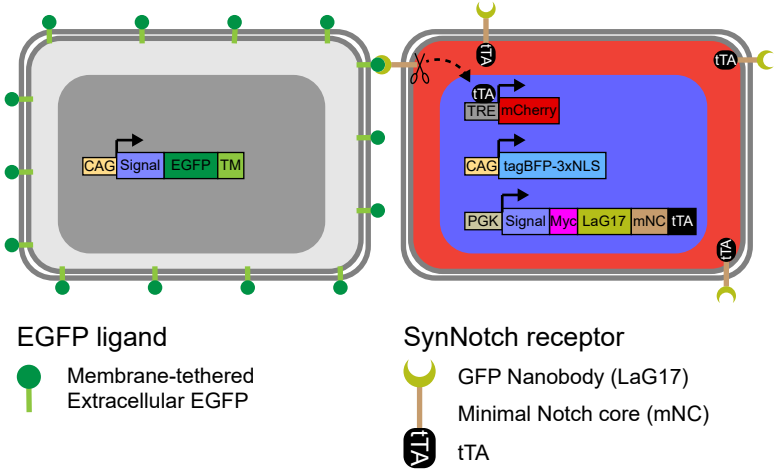

FIGURE 2

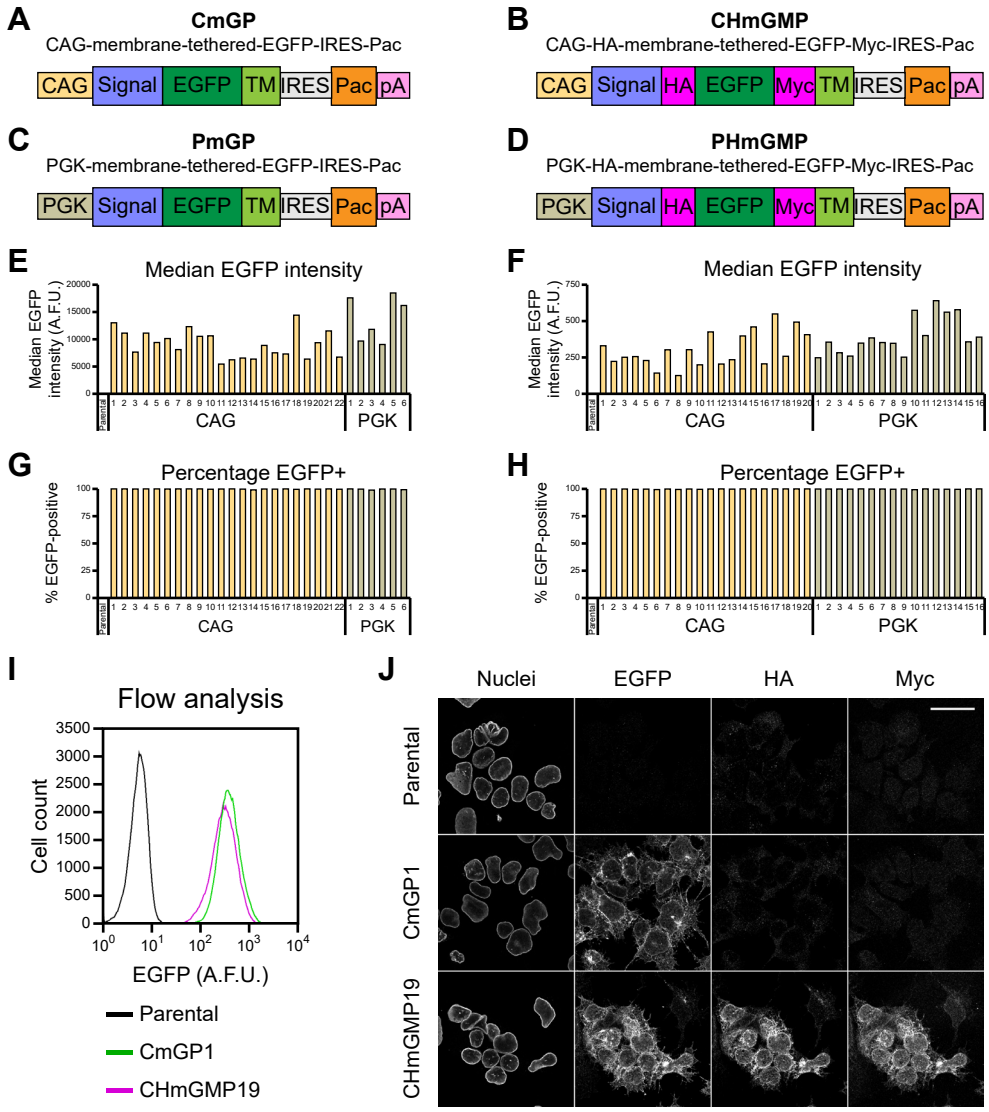
A
CmGP
CAG-membrane-tethered-EGFP-IRES-Pac
CAG Signal EGFP TM IRES Pac pA
B
CHmGMP
CAG-HA-membrane-tethered-EGFP-Myc-IRES-Pac
CAG Signal HA EGFP Myc TM IRES Pac pA
C
PmGP
PGK-membrane-tethered-EGFP-IRES-Pac
PGK Signal EGFP TM IRES Pac pA
D
PHmGMP
PGK-HA-membrane-tethered-EGFP-Myc-IRES-Pac
PGK Signal HA EGFP Myc TM IRES Pac pA
E
Median EGFP intensity
Median EGFP intensity (A.F.U.)
Parental
CAG
PGK
F
Median EGFP intensity
Median EGFP intensity (A.F.U.)
Parental
CAG
PGK
G
Percentage EGFP+
% EGFP-positive
Parental
CAG
PGK
H
Percentage EGFP+
% EGFP-positive
Parental
CAG
PGK
I
Flow analysis
Cell count
EGFP (A.F.U.)
Parental
CmGP1
CHmGMP19
J
Nuclei
EGFP
HA
Myc
Parental
CmGP1
CHmGMP19

FIGURE 3

A

STC receiver cells (SynNotch-TRE-mCherry)

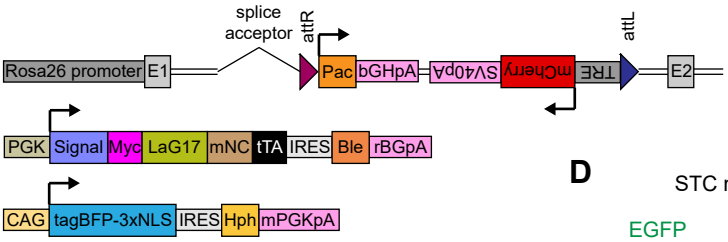

B

Wild-type

C

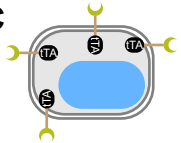

EV control "receivers"

Flow analysis of EGFP- cells

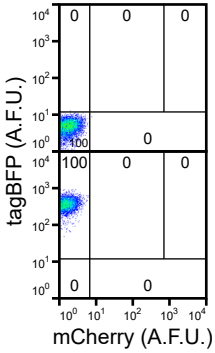

D

STC receivers + CmGP1 senders

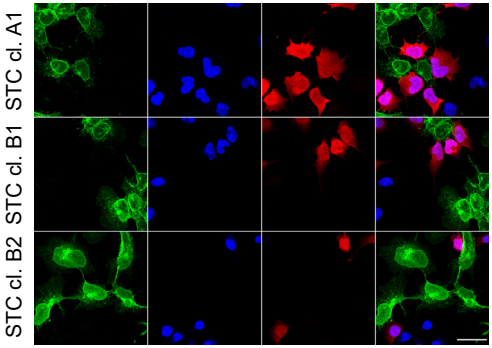

E

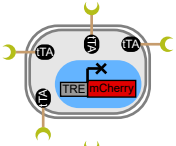

STC receivers

F

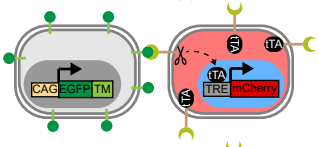

STC receivers + CmGP1 senders

G

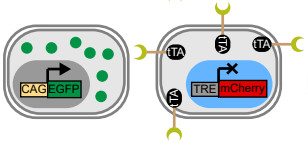

STC receivers + E14GIP1 "senders"

H

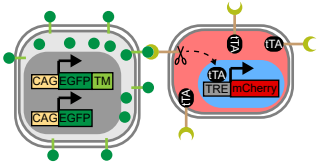

STC receivers + CmGP1GH1 senders

Flow analysis of tagBFP+ EGFP- cells

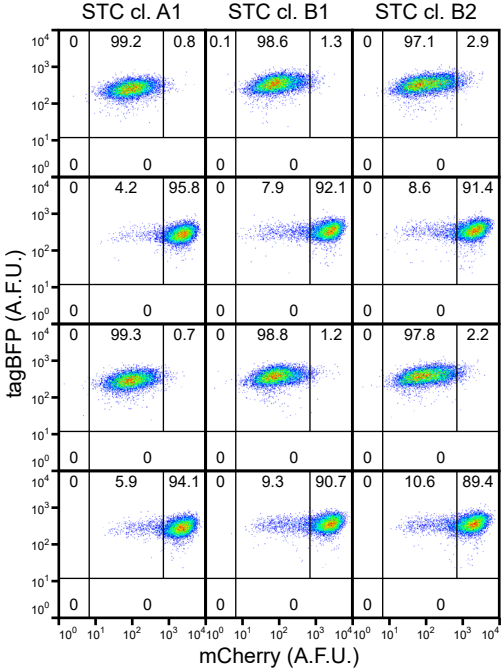

FIGURE 4

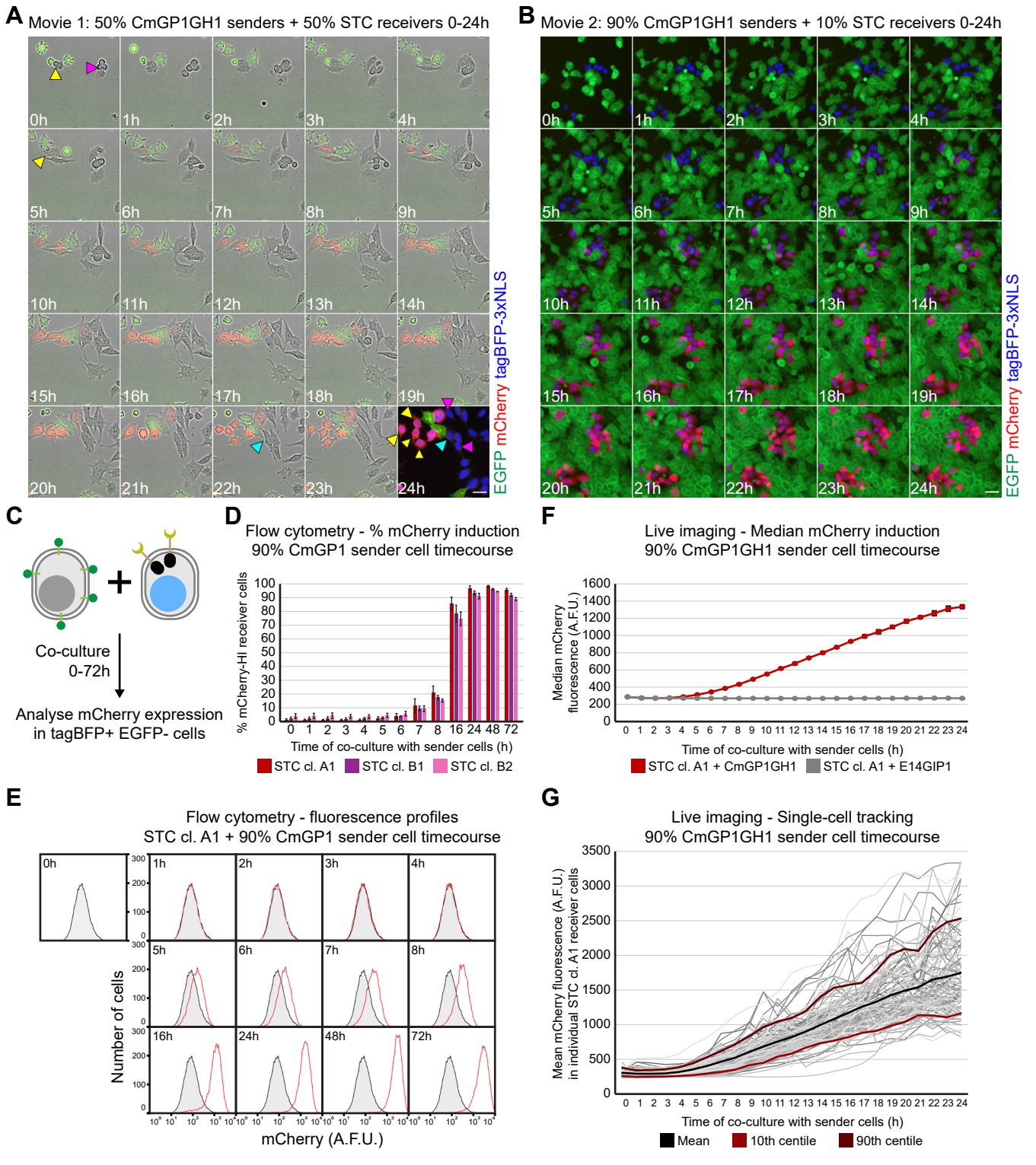
A
Movie 1: 50% CmGP1GH1 senders + 50% STC receivers 0-24h
0h
1h
2h
3h
4h
5h
6h
7h
8h
9h
10h
11h
12h
13h
14h
15h
16h
17h
18h
19h
20h
21h
22h
23h
24h
EGFP mCherry tagBFP-3xNLS
B
Movie 2: 90% CmGP1GH1 senders + 10% STC receivers 0-24h
EGFP mCherry tagBFP-3xNLS
C
Co-culture
0-72h
Analyse mCherry expression
in tagBFP+ EGFP- cells
D
Flow cytometry - % mCherry induction
90% CmGP1 sender cell timecourse
% mCherry-HI receiver cells
Time of co-culture with sender cells (h)
STC cl. A1
STC cl. B1
STC cl. B2
F
Live imaging - Median mCherry induction
90% CmGP1GH1 sender cell timecourse
Median mCherry
fluorescence (A.F.U.)
Time of co-culture with sender cells (h)
STC cl. A1 + CmGP1GH1
STC cl. A1 + E14GIP1
E
Flow cytometry - fluorescence profiles
STC cl. A1 + 90% CmGP1 sender cell timecourse
Number of cells
mCherry (A.F.U.)
G
Live imaging - Single-cell tracking
90% CmGP1GH1 sender cell timecourse
Mean mCherry fluorescence (A.F.U.)
in individual STC cl. A1 receiver cells
Time of co-culture with sender cells (h)
Mean
10th centile
90th centile

FIGURE 5

A Movie 3: 50% CmGP1GH1 senders + 50% STC receivers 0-24h

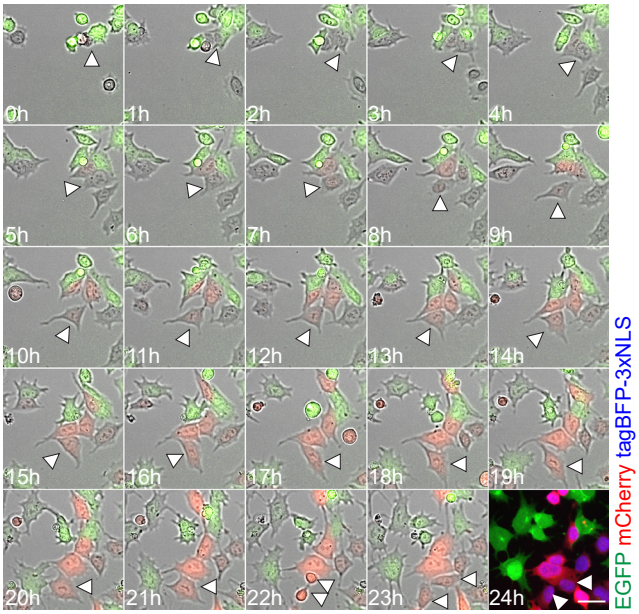

B

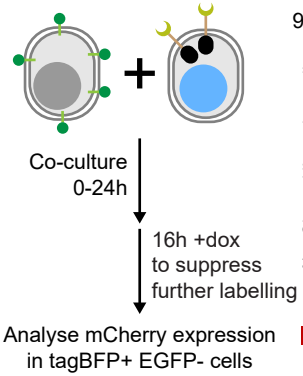

C

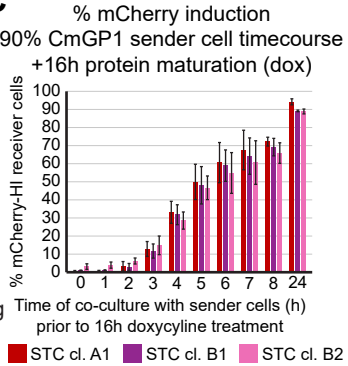

D

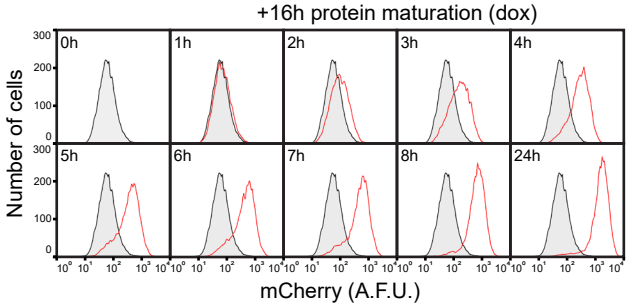

Timepoints refer to initial duration of dox-free co-culture permissive for mCherry induction prior to addition of dox for 16h

FIGURE 6

A

Chimaeric blastocysts with STC receiver + CmGP1GH1 sender cells

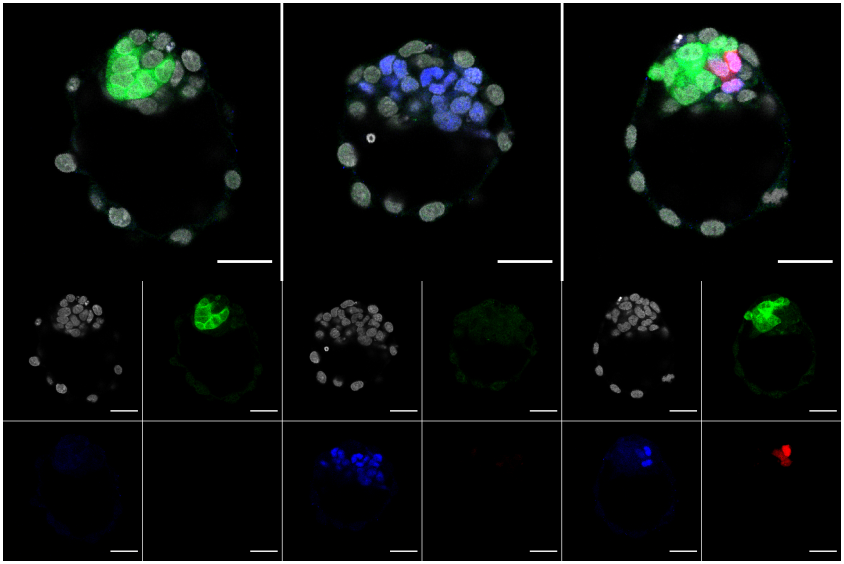

Nuclei EGFP tagBFP-3xNLS mCherry

B

	mCherry-HI embryos / total embryos			
	All clones	STC cl. A1	STC cl. B1	STC cl. B2
Wild-type	**0/11**	-	-	-
Senders only	**0/27**	-	-	-
Receivers only	**1/19**	1/13	0/3	0/3
Receivers+senders	**80/80**	56/56	23/23	11/11

FIGURE 7

A

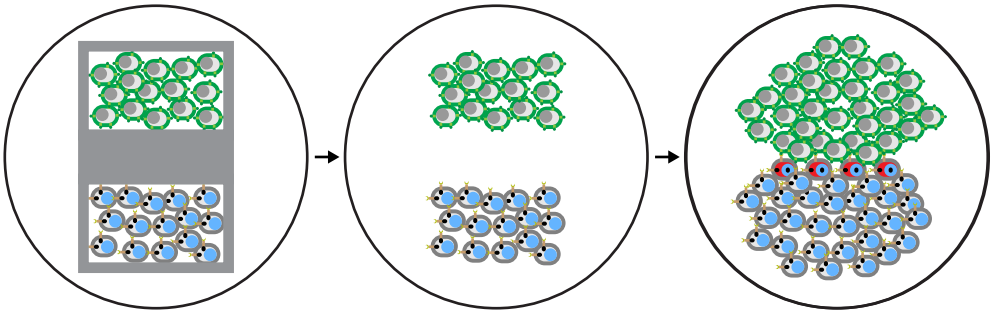

Plate sender and receiver cells in separate wells of multiwell insert

Remove multiwell insert
Give cells time to proliferate

Transgene expression induced at linear interface between sender and receiver cells

B

mCherry induction in STC receivers at sender-receiver border

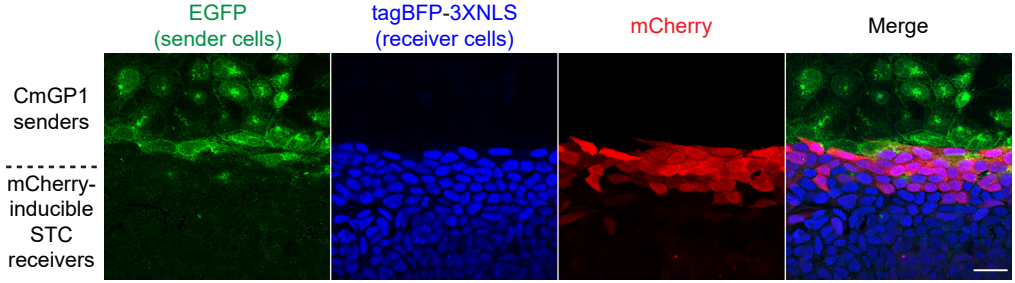

C

STN receiver cells (Neurog1-inducible)

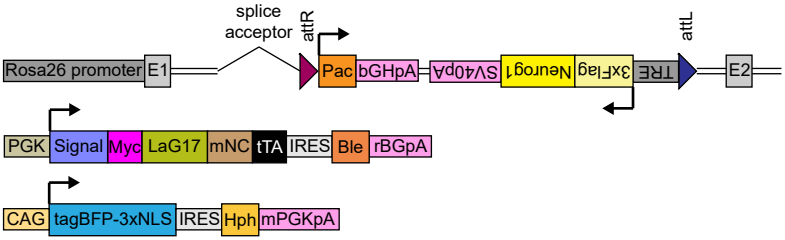

D
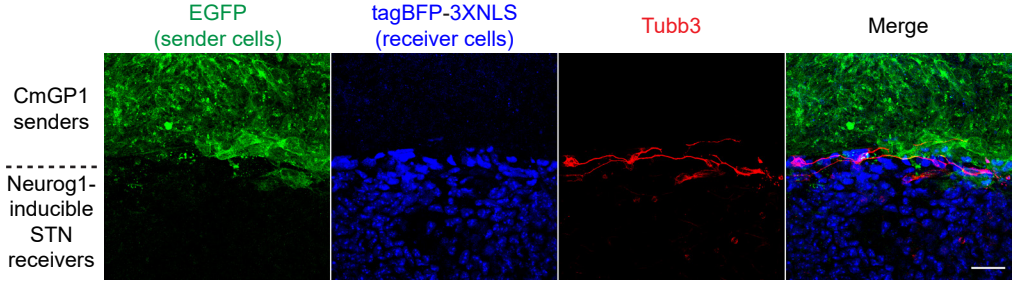
Forced neuronal differentiation of STN receivers at sender-receiver border